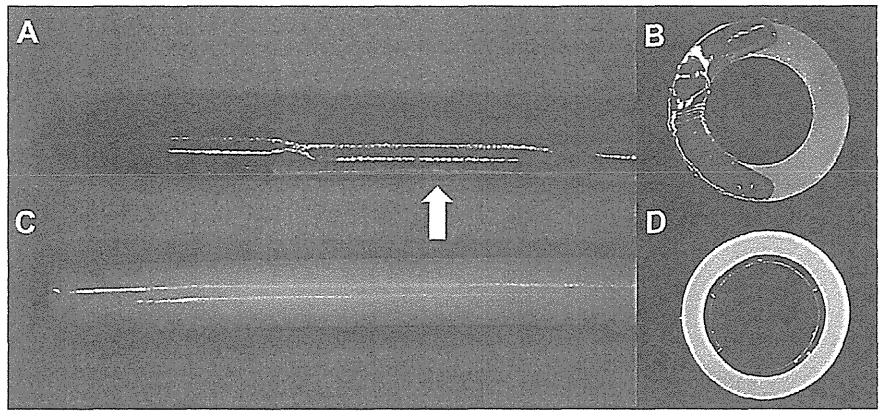

Fig. 1. Specification of the catheters: Tip shapes and cross section. A: The tip of the Groshong catheter is a closed semi-round tip. The arrow indicates the side slits valve. B: The cross section of the Groshong catheter 4Fr. Outer diameter is 1.427 mm and inner diameter is 0.858 mm (measured). C: The tip of PI Catheter is a simple open-end. D: The cross section of the PI Catheter 4Fr. Outer diameter is 1.327 mm and inner diameter is 0.860 mm (measured).

brachial veins occlusion therefore required traditional CVC insertion from the jugular vein. They included a female and 25 male patients, with age ranging from 58 to 80 years (median 65.5 years). The most common underlying indication was chemotherapy or chemo-radiotherapy for advanced esophageal cancer, accounting for 96% of our total study population. The remaining reason of one case was a requirement of nutritional support due to prolonged postoperative leakage after total gastrectomy. No hematoma developed at the puncture sites in all patients during the procedures. There were no statistically significant differences in the patient demographics, included primary indication for PICC placement between Groshong and PI Catheter groups. Similarly, no significant differences in the arm used, insertion location, tip location, and duration of PICC placement, were noted (Table 3).

The median catheter dwell time was 16 days (range, 9–39 days) for Groshong and 16 days (range, 5–52 days) for PI Catheter ($p = 0.9928$). No difference was seen in either completion rate of PICC indication (81.8% vs. 92.9%, $p = 0.5648$), nor total complication rate (9.1% vs. 14.3%, $p = 1.0000$) between the two groups.

Three cases were not able to complete their primary indications of PICCs placement, 2 in Groshong and 1 in PI Catheter group, respectively. In 2 cases in Groshong group, CR-BSI was suspected and the catheters were prematurely removed. There was no thrombus at the tip and the culture results were negative although one case alleviated fever immediately after the removal. In remaining 1 case in PI Catheter group, a significant catheter occlusion with thrombus was observed and a catheter was re-inserted at the opposite arm.

In addition to one case requiring premature removal, another case presented complete occlusion of the catheter in PI Catheter group. Totally 2 out of 14 (14.3%) cases showed catheter occlusion in PI Catheter Group, whereas none in Groshong ($p = 0.4867$).

A phlebitis was noted in 1 case in each group, respectively ($p = 1.000$). And both cases complained of a slight rubor and negligible pain to along a catheter dwelling vein. Within one day, those symptoms disappeared by acrinol poultice or cooling. All patients are examined by enhanced computed tomography for their disease but any thrombus in the peripheral and central veins was not pointed out (data not shown).

Post-procedural hemorrhage was noted in 8 patients in Groshong group and 12 patients in PI Catheter group, respectively ($p = 0.2026$). And hemorrhage for duration of PICC was noted in 3 patients in Groshong group and 4 in PI Catheter group. Most of them were minimal bleeding spontaneously controlled. Post-remove hemorrhage was noted in 5 patients in Groshong group and no patients in PI Catheter group, respectively and there is significant difference ($p = 0.0017$). (Table 4)

Table 2
The characteristics of catheters.

	Groshong Catheter	PI Catheter
Size	4Fr	4Fr
Lumen	Single	Single
Material	Silicone	Polyurethane
Tip design	Closed semi-round tip	Simple, open end
Valve system	Three way "Groshong valves"	–
Outer diameter[a]	1.427 mm	1.327 mm
Inner diameter[a]	0.858 mm	0.860 mm
Fixed price[b]	16,000 yen	12,000 yen
Manufacturer	Bard	Covidien

[a] Outer and inner diameter are measured for this study.
[b] Fixed prices of the catheters are in Japanese Yen.

4. Discussion

Our study showed no significant difference in the completion rate of PICC indication between the two different catheters in

Table 3
Patient demographics, primary indications for PICC[a] placement and procedural data.

	Groshong	PI Catheter	*p* value
Registry case	12	14	
Placed case	11	14	0.462
Gender			1.000
Male/ female	11/0	13/1	
Age			
Median (range)	67 (58–80)	64.5 (56–80)	0.693
Catheter dwell time (days)			
Median (range)	16 (9–39)	16 (5–52)	0.993
Primary indication for PICC[a]			1.000
Chemo or chemoradiotherapy	11	13	
Total parenteral nutrition	0	1	
Arm used			0.434
Right	5	4	
Left	6	10	
Insertion location			0.689
Antebrachial region	2	2	
Elbow portion	1	3	
Brachial region	8	9	
Catheter tip placement			1.0000
Superior vena cava	11/0	14/0	

[a] PICC: Peripherally inserted central venous catheter.

Table 4
Completion of Therapy and Complications.

	Groshong ($n = 11$)	PI Catheter ($n = 14$)	p value
The completion of PICC[a] indication			
Yes	9	13	0.565
Total complications	**2**	**2**	1.000
Phlebitis	1	1	1.000
Vein thrombosis	0	0	1.000
Blood stream infection	1	0	0.440
Occlusion	0	2[c]	0.487
Hemorrhage[b] at site of insertion			
Post-procedural	8	12	0.623
Duration of PICC placement	3	4	1.000
Post-removal	5	0	0.008
Complaint of site of insertion and a brachial region.			
Yes	2	1	0.565

[a] PICC: Peripherally inserted central venous catheter.
[b] The hemorrhage with pressure hemostasis required or coagulation in a dressing materials.
[c] Two occlusion cases were observed by PI Catheter, one case of them was observed on the date of the scheduled to remove, and was reported as a case which completed the indication.

gastrointestinal surgical patients. However, PI Catheter was associated with a significantly higher incidence of catheter occlusion, and Groshong was associated with a significantly higher incidence of hemorrhages after catheter removal. To our knowledge, there are no previous studies comparing performances of these two widely used PICC catheters.

As for traditional CVCs, Linder et al reported that no significant differences were found between the silicon and polyurethane catheters regarding the number and size of radiologic thrombi in the peripheral and central veins, catheter occlusion rate, and platelet adhesion to the inner side of the catheter tip at removal.[20] In our study, all patients were examined by enhanced computed tomography for their own disease within one month after removal, and any thrombus in the peripheral and central veins was not diagnosed. The thrombus formation in a catheter relates to development of CR-BSI.[21,22] In hemodialysis patients, the rate of thrombus formation in the group with CR-BSI has been reported to be three times higher as compared with the group without CR-BSI.[23] A heparin administration as prophylaxis has been thus recommended.[24,25] In our study, 2 cases with thrombus formation in a catheter were observed, only in PI Catheter group but there is statically no significant difference. As described in the report by Hoffer et al[26] (Table 5), hypothetically this might be related to the absence of valve system rather than the difference in the material of the catheters. And the association of a thrombus formation and a blood stream infection was not recognized in this study.

Although PICC has been reported to be associated with lower incidence of phlebitis and DVT compared to traditional CVCs,[15] blood flow through the brachial vein is less than that through the other central veins such as the subclavian or internal jugular. This feature, also in view of the smaller size of the vessel, and therefore the relatively larger intraluminal occupation, should be considered the main predisposing factor for PICC-related thrombosis. Groove et al. reported larger PICC diameter to be predictive of DVT.[27] Simulation with annular flow model, PICCs by the insertion of a centrally located obstruction in a vein, dramatically decreased blood flow rates by as much as 93%.[28] According to the adhesion model based on the JKR (Johnson, Kendall and Roberts) model theory,[29] frictional and adhesion parameters between vein against silicone and polyurethane were reported by Prokopovich et al. The adhesive friction of vein to the silicone surface was more dominant than to polyurethane.[30] Based on the previous study of comparing the silicone PICCs with a distal valve, and the polyurethane PICCs with a proximal valve, significantly higher incidences of phlebitis (23.2% versus 11.6%, $P = 0.003$) and CR-BSI (6.2% versus 2%, $P = 0.043$) were noted in the silicone PICCs.[31] And the similar tendency in incidence of phlebitis/CR-BSI was seen in both our study and the trial by Hoffer et al.[32] We have to recognize that the dwelling PICC in a vein is a very dangerous situation which can cause a thrombosis and CR-BSI. The low angiopathy polyurethane which can make an outer diameter small for obtaining the flow is more advantageous. Despite these data, we found no difference in phlebitis and DVT between two catheters. For this reason, the number of enrolled cases is small. In order to prove this, the further case accumulation will be required.

More significant hemorrhage was observed in Groshong group than in PI Catheter group after catheter removal significantly. The contact reaction of a catheter with subcutaneous tissue might be one cause. More post-procedural hemorrhage was also observed in Groshong group, but not significantly. The difference in hardness and outer diameter could be also partially responsible for these differences.

As listed in Table 5, to our knowledge, only 3 trials were reported previously. Besides our study, three of 4 trials that compared silicon and polyurethane revealed the inferiority in durability in silicon catheter. Hoffer et al.[32] reported that fracture (i.e. partial or total disruption of catheter) was observed more frequently in silicon catheter group. Similar tendency was also reported by Ong et al.[31]

Probably, although the further case accumulation is required, since there is no difference of both catheters, the standpoint of medical economics will recommend a cheaper catheter.

In conclusion, our study showed no significant difference in the completion rates of indication between a silicone catheter with distal side slits and a polyurethane catheter with open-end tip. A polyurethane catheter with open-end tip was associated with higher incidence of catheter occlusion, whereas a silicone catheter with distal side slits was associated with more significant hemorrhages at removal. A continuous accumulation of clinical cases is necessary to further clarify differences in performance of these two products in gastrointestinal surgical patients.

Table 5
Randomized controlled trial comparing peripherally inserted central venous Catheters.

Author	Year	Cases	Size, lumens	Valve	Material	Phlebitis	CR-BSI[b]	Occlusion	Fracture
Hoffer[26]	1999	180	5Fr, single	P	Polyurethane	0.5%	5.8%	3.3%	1.6%
		182	5Fr, single	None	Polyurethane	0.0%	5.8%	7.1%	1.1%
Hoffer[32]	2001	48	4Fr, single	D	Silicone	1.9%	8.3%	14.6%	35.4%[a]
		52	4Fr, single	P	Polyurethane	0.0%	1.9%	9.6%	5.8%[a]
Ong[31]	2010	194	4Fr, single	D	Silicone	23.2%[a]	6.2%[a]	11.9%	3.6%
		198	4Fr, single	P	Polyurethane	11.6%[a]	2.0%[a]	9.6%	1.0%
Present Study	2011	12	4Fr, single	D	Silicone	9.1%	9.1%	0.0%	0.0%
		14	4Fr, single	None	Polyurethane	7.1%	0.0%	14.3%	0.0%

Valve type: D; distal side slits valve (Groshong® valve), P; proximal valve (PASV® Valve).
[a] p value was reported significant (<0.05).
[b] Catheter related blood stream infection.

Statement of authorship

Hiromichi Miyagaki M.D. carried out the studies and data analyses, and drafted the manuscript. Kiyokazu Nakajima M.D. conceived of the study, participated in its design and coordination and drafted the manuscript. Joji Hara M.D. participated in this study design, carried out the studies and collection of data. Makoto Yamasaki M.D., Yukinori Kurokawa M.D., Hiroshi Miyata M.D. Shuji Yoshiyuki Fujiwara M.D. Takiguchi M.D. Prof. Masaki Mori and Yuichiro Doki M.D. are participated in provision of significance advice and consultation.

Conflict of interest

This study was supported financially by Nippon Sherwood Medical Industries Ltd. (Tokyo, Japan). The authors declare no further conflict of interest.

Acknowledgements

The authors wish to thank all attending doctors and nurses who participated in this study, and also thank all colleagues who advised us in carrying this study.

References

1. Merrer J, De Jonghe B, Golliot F, Lefrant JY, Raffy B, Barre E, et al. Complications of femoral and subclavian venous catheterization in critically ill patients: a randomized controlled trial. *Jama* 2001;**286**:700–7.
2. McGee DC, Gould MK. Preventing complications of central venous catheterization. *N Engl J Med* 2003;**348**:1123–33.
3. Ayas NT, Norena M, Wong H, Chittock D, Dodek PM. Pneumothorax after insertion of central venous catheters in the intensive care unit: association with month of year and week of month. *Qual Saf Health Care* 2007;**16**:252–5.
4. Eisen LA, Narasimhan M, Berger JS, Mayo PH, Rosen MJ, Schneider RF. Mechanical complications of central venous catheters. *J Intensive Care Med* 2006;**21**:40–6.
5. Leung TK, Lee CM, Tai CJ, Liang YL, Lin CC. A retrospective study on the long-term placement of peripherally inserted central catheters and the importance of nursing care and education. *Cancer Nurs* 2011;**34**:E25–30.
6. Ryder MA. Peripheral access options. *Surg Oncol Clin N Am* 1995;**4**:395–427.
7. Smith JR, Friedell ML, Cheatham ML, Martin SP, Cohen MJ, Horowitz JD. Peripherally inserted central catheters revisited. *Am J Surg* 1998;**176**:208–11.
8. Ng PK, Ault MJ, Ellrodt AG, Maldonado L. Peripherally inserted central catheters in general medicine. *Mayo Clin Proc* 1997;**72**:225–33.
9. Hadaway LC. Major thrombotic and nonthrombotic complications. Loss of patency. *J Intraven Nurs* 1998;**21**:S143–60.
10. Skiest DJ, Abbott M, Keiser P. Peripherally inserted central catheters in patients with AIDS are associated with a low infection rate. *Clin Infect Dis* 2000;**30**:949–52.
11. Kovacevich DS, Papke LF. Guidelines for the prevention of intravascular catheter-related infections: Centers for Disease Control and Prevention. *Nutr Clin Pract* 2003;**18**:95–6.
12. Haider G, Kumar S, Salam B, Masood N, Jamal A, Rasheed YA. Determination of complication rate of PICC lines in oncological patients. *J Pak Med Assoc* 2009;**59**:663–7.
13. Cowl CT, Weinstock JV, Al-Jurf A, Ephgrave K, Murray JA, Dillon K. Complications and cost associated with parenteral nutrition delivered to hospitalized patients through either subclavian or peripherally-inserted central catheters. *Clin Nutr* 2000;**19**:237–43.
14. King MM, Rasnake MS, Rodriguez RG, Riley NJ, Stamm JA. Peripherally inserted central venous catheter-associated thrombosis: retrospective analysis of clinical risk factors in adult patients. *South Med J* 2006;**99**:1073–7.
15. Bonizzoli M, Batacchi S, Cianchi G, Zagli G, Lapi F, Tucci V, et al. Peripherally inserted central venous catheters and central venous catheters related thrombosis in post-critical patients. *Intensive Care Med* 2011;**37**:284–9.
16. Mazzola JR, Schott-Baer D, Addy L. Clinical factors associated with the development of phlebitis after insertion of a peripherally inserted central catheter. *J Intraven Nurs* 1999;**22**:36–42.
17. Chow LM, Friedman JN, Macarthur C, Restrepo R, Temple M, Chait PG, et al. Peripherally inserted central catheter (PICC) fracture and embolization in the pediatric population. *J Pediatr* 2003;**142**:141–4.
18. Kothari D, Gupta S, Tandon N, Mehrotra A. Accidental cut of peripherally inserted central venous catheter. *Intensive Care Med* 2010;**36**:2154–5.
19. Maki DG, Botticelli JT, LeRoy ML, Thielke TS. Prospective study of replacing administration sets for intravenous therapy at 48- vs 72-hour intervals. 72 hours is safe and cost-effective. *Jama* 1987;**258**:1777–81.
20. Linder LE, Curelaru I, Gustavsson B, Hansson HA, Stenqvist O, Wojciechowski J. Material thrombogenicity in central venous catheterization: a comparison between soft, antebrachial catheters of silicone elastomer and polyurethane. *JPEN J Parenter Enteral Nutr* 1984;**8**:399–406.
21. Raad II , Luna M, Khalil SA, Costerton JW, Lam C, Bodey GP. The relationship between the thrombotic and infectious complications of central venous catheters. *Jama* 1994;**271**:1014–6.
22. Timsit JF, Farkas JC, Boyer JM, Martin JB, Misset B, Renaud B, et al. Central vein catheter-related thrombosis in intensive care patients: incidence, risks factors, and relationship with catheter-related sepsis. *Chest* 1998;**114**:207–13.
23. Hernandez D, Diaz F, Suria S, Machado M, Lorenzo V, Losada M, et al. Subclavian catheter-related infection is a major risk factor for the late development of subclavian vein stenosis. *Nephrol Dial Transplant* 1993;**8**:227–30.
24. Randolph AG, Cook DJ, Gonzales CA, Andrew M. Benefit of heparin in peripheral venous and arterial catheters: systematic review and meta-analysis of randomised controlled trials. *Bmj* 1998;**316**:969–75.
25. Elliott TS, Curran A. Effects of heparin and chlorbutol on bacterial colonisation of intravascular cannulae in an in vitro model. *J Hosp Infect* 1989;**14**:193–200.
26. Hoffer EK, Borsa J, Santulli P, Bloch R, Fontaine AB. Prospective randomized comparison of valved versus nonvalved peripherally inserted central vein catheters. *AJR Am J Roentgenol* 1999;**173**:1393–8.
27. Grove JR, Pevec WC. Venous thrombosis related to peripherally inserted central catheters. *J Vasc Interv Radiol* 2000;**11**:837–40.
28. Nifong TP, McDevitt TJ. The effect of catheter to vein ratio on blood flow rates in a simulated model of peripherally inserted central venous catheters. *Chest*; 2011.
29. Johnson KL, Kendall K, Roberts AD. Surface energy and the contact of Elastic Solids. *Proc R Soc Lond Ser A* 1971;**324**:301–13.
30. Prokopovich P, Perni S. Prediction of the frictional behavior of mammalian tissues against biomaterials. *Acta Biomater* 2010;**6**:4052–9.
31. Ong CK, Venkatesh SK, Lau GB, Wang SC. Prospective randomized comparative evaluation of proximal valve polyurethane and distal valve silicone peripherally inserted central catheters. *J Vasc Interv Radiol* 2010;**21**:1191–6.
32. Hoffer EK, Bloch RD, Borsa JJ, Santulli P, Fontaine AB, Francoeur N. Peripherally inserted central catheters with distal versus proximal valves: prospective randomized trial. *J Vasc Interv Radiol* 2001;**12**:1173–7.

UICC
global cancer control

IJC
International Journal of Cancer

IGFBP7 downregulation is associated with tumor progression and clinical outcome in hepatocellular carcinoma

Yoshito Tomimaru[1], Hidetoshi Eguchi[1], Hiroshi Wada[1], Shogo Kobayashi[1], Shigeru Marubashi[1], Masahiro Tanemura[1], Koji Umeshita[2], Tonsok Kim[3], Kenichi Wakasa[4], Yuichiro Doki[1], Masaki Mori[1] and Hiroaki Nagano[1]

[1] Department of Surgery, Graduate School of Medicine, Osaka University, Osaka, Japan
[2] Division of Health Sciences, Graduate School of Medicine, Osaka University, Osaka, Japan
[3] Department of Radiology, Graduate School of Medicine, Osaka University, Osaka, Japan
[4] Department of Pathology, Osaka City University Hospital, Osaka, Japan

Insulin-like growth factor-binding protein 7 (IGFBP7) functions in several cellular processes including proliferation, senescence and apoptosis. This study analyzed IGFBP7 function in hepatocellular carcinoma (HCC) cells by gene manipulation and investigated the prognostic significance of IGFBP7 expression in clinical HCC samples. In this study, we investigated changes in malignant potential such as cell growth and invasiveness in an HCC cell line, PLC/PRF/5, after transfection with shRNA against *IGFBP7*. The extent of apoptosis and cell cycle progression were examined after the transfection. The correlation between immunohistochemically determined IGFBP7 expression and long-term postoperative prognosis after curative resection was also investigated in clinical HCC specimens obtained from 104 patients. PLC/PRF/5 cells transfected with shRNA against *IGFBP7* showed significantly more rapid growth and stronger invasiveness than control cells. Annexin V assays showed that the IGFBP7-depleted cells were significantly more resistant to apoptosis than the control cells, and showed decreased expression of cleaved caspase-3 and PARP. Cell cycle progression was more rapid in the IGFBP7-suppressed cells. In clinical HCC specimens, IGFBP7 expression was judged as positive in 67 patients (64.4%) and negative in the remaining 37 patients (35.6%). The IGFBP7 downregulation correlated significantly with poor postoperative prognosis, and IGFBP7 status was identified as an independent significant prognostic factor. Our results indicated that IGFBP7 expression correlated significantly with the malignant potential in HCC cells, suggesting that the expression could be a useful prognostic marker for HCC.

Hepatocellular carcinoma (HCC) is a common malignancy worldwide, but especially in Japan and other East Asian countries.[1,2] Although surgery plays a major role in the treatment of HCC, less than 30% of patients with HCC are surgical candidates owing to limiting factors such as severe impairment of reserve hepatic function, bilobar tumor distribution and extrahepatic metastasis. Additionally, no effective chemotherapy regimens have been established for treating HCC.[3] Thus, no effective therapy can be offered in many cases of HCC. Such dismal prognosis is not always predicted by conventional prognostic indicators such as vascular invasion, tumor multiplicity and tumor size.[4–6] New indicators are thus clearly needed.

Insulin-like growth factor binding protein 7 (IGFBP7), which is also known as IGFBP-rP1 and MAC25, has been implicated in several cellular processes such as proliferation, senescence and apoptosis. IGFBP7 also shows tumor suppressive activity through the induction of apoptosis and it is downregulated in some cancers.[7–13] In addition, several studies found a significant association between IGFBP7 and not only apoptosis, but also prognosis, in some kinds of cancers including colorectal and breast cancer.[14,15] However, the functional significance of IGFBP7 in HCC remains unclear.

This study analyzed the function of IGFBP7 in HCC cells in gene manipulation experiments, and investigated the prognostic significance of IGFBP7 expression in clinical HCC samples by immunohistochemical analysis of resected specimens.

Key words: hepatocellular carcinoma (HCC), insulin-like growth factor binding protein 7 (IGFBP7), apoptosis

Abbreviations: 95% CI: 95% confidence interval; AFP: alpha-fetoprotein; Anti-HCV Ab: anti-hepatic C virus antibody; DFS: disease-free survival; HBs-Ag: hepatitis B surface antigen; HCC: hepatocellular carcinoma; IGFBP7: insulin-like growth factor binding protein 7; OR: odds ratio; OS: overall survival; PBGD: porphobilinogen deaminase; pERK: phoshorylated ERK; PI: propidium iodide; PIVKA-II: protein induced by vitamin K absence or antagonists-II; qRT-PCR: quantitative reverse transcription-polymerase chain reaction; shRNA: short hairpin RNA

DOI: 10.1002/ijc.25994
History: Received 6 Sep 2010; Accepted 2 Feb 2011; Online 16 Feb 2011

Correspondence to: Hiroaki Nagano, M.D., Ph.D., Department of Surgery, Graduate School of Medicine, Osaka University, 2-2 Yamadaoka E-2, Suita 565-0871 Osaka, Japan, Tel.: +81-6-6879-3251; Fax: +81-6-6879-3259, E-mail: hnagano@gesurg.med.osaka-u.ac.jp

Material and Methods

HCC cell lines and clinical tissue specimens

Four human HCC cell lines, PLC/PRF/5, HuH7, HLE and HepG2 were obtained from the Japan Cancer Research

Resources Bank (Tokyo, Japan). These cells were maintained in Dulbecco's modified Eagle's medium supplemented with 10% fetal bovine serum, 100 U/ml penicillin and 100 mg/ml streptomycin at 37°C in a humidified incubator with 5% CO_2 in air.

Surgical specimens were obtained from 104 patients with HCC who underwent curative hepatic resection in the Osaka University Hospital from 2000 to 2007 after informed consent in accordance with the institutional ethical guidelines of Osaka University. Curative resection was defined as complete removal of all macroscopically evident tumors. Patients who underwent transarterial chemoembolization preoperatively were excluded from this study. After hepatic resection, the patients were followed up at regular intervals of 3–4 months with physical examination, assaying of tumor markers including alpha-fetoprotein (AFP) and protein induced by vitamin K absence or antagonists-II (PIVKA-II), liver biochemistry testing, abdominal ultrasonography and abdominal computed tomography. The median duration of clinical follow-up after the initial hepatectomy was 3.5 ± 2.3 years.

Drugs and reagents

A polyclonal goat anti-human IGFBP7 antibody and polyclonal rabbit anti-human IGFBP7 antibody (Santa Cruz Biotechnology, Santa Cruz, CA) was used for immunohistochemistry and western blot analysis, respectively. Antibodies to caspase-3, cleaved caspase-3, PARP, cleaved PARP, ERK, phoshorylated ERK (pERK), cyclin D1 and p27 were purchased from Cell Signaling Technology (Beverly, MA), antibodies to cyclin E and p21 were purchased from Santa Cruz Biotechnology, and an antibody to actin was purchased from Sigma-Aldrich Co. (Louis, MO).

Plasmids and transfection

Plasmid coding for short hairpin RNA (shRNA) against *IGFBP7* and *IGFBP7* expression plasmid were purchased from OriGene Technologies (Rockville, MD) and used to transfect HCC cells using Lipofectamine 2000 (Invitrogen, Carlsbad, CA) according to the instructions provided by the manufacturer. After transfection of the shRNA plasmid and the *IGFBP7* expression plasmid into the HCC cells for 24 hr, stable transfectants were selected and maintained in 1.0 μg/ml of puromycin (Sigma-Aldrich, St. Louis, MO) and 600 μg/ml of G418 (Gibco-BRL, Grand Island, NY), respectively. The control vector plasmid expressing non-effective shRNA was similarly introduced into cells to establish negative control cells for the shRNA plasmid experiments. Empty vector plasmid was also similarly used to establish negative control cells for the *IGFBP7* expression plasmid for the *IGFBP7* expression plasmid experiments.

Cell proliferation assay

Cells were uniformly seeded (4×10^4/well for PLC/PRF/5 and 2×10^4/well for HuH7) in triplicates into 24-well dishes (Day 0). Cells were counted using a CellTac kit (Nihon Koden, Tokyo, Japan) on Days 1–5.

Real-time quantitative reverse transcription-polymerase chain reaction

Total RNA isolated from cells was prepared using TRIzol reagent (Invitrogen), and reverse transcription was performed with SuperScript II (Invitrogen) based on the protocols supplied by the manufacturer. Real-time quantitative reverse transcription-polymerase chain reaction (qRT-PCR) was performed using the Light Cycler (Roche Diagnostics, Mannheim, Germany), and the amount of target gene expression was calculated. The expression of the target gene was normalized relative to the expression of *porphobilinogen deaminase* (*PBGD*), which was used as an internal control. The designed PCR primers were as follows; *IGFBP7* forward primer; 5′-CTGGGTGCTGGTATCTCCTC-3′; *IGFBP7* reverse primer; 5′-TATAGCTCGGCACCTTCACC-3′; *SMARCB1* forward primer; 5′-TCTGGATTTGAACCCGCTGA-3′; *SMARCB1* reverse primer; 5′-TGCTGTATGCGATGGTGGTG-3′; *BNIP3L* forward primer; 5′-CGGACTCGGCTTGTTGTGTT-3′; *BNIP3L* reverse primer; 5′-ATGGGTAGCTCCACCCA GGA-3′; *PBGD* forward primer; 5′-TGTCTGGTAACGGC AATGCGGCTGCAAC-3′; *PBGD* reverse primer; 5′-TCAA TGTTGCCACCACACTGTCCGTCT-3′

Western blot analysis

Cells grown to semiconfluence were washed and collected with a rubber scraper. After centrifugation, the cell pellets were resuspended, and the extracts were centrifuged and the supernatant fraction was collected. Western blot analysis was carried out as described previously.[16,17] The expression of the target protein was evaluated by comparison to the expression of actin.

Annexin V assay

The binding of annexin V was used here as a sensitive assessment of apoptosis, as described previously.[17,18] Cells were stained by Annexin V-APC and propidium iodide (PI) (BD Biosciences, Franklin Lakes, NJ), and analyzed on a FACS Aria (BD Biosciences).

Invasion assay

The invasion assay was performed using transwell culture chambers (BD Biosciences) according to the instructions provided by the manufacturer. The upper chamber was loaded with cell suspension and the lower chamber was loaded with 10% FBS. After incubation (48 hr for PLC/PRF/5 and 24 hr for HuH7), cells that had invaded the undersurface of the membrane were counted under a microscope. Four microscopic fields were randomly selected for cell counting.

Cell cycle analysis

Cell cycle analysis was performed based on flow cytometric analysis, as described previously.[19] Briefly, cells were washed and fixed. PI and RNase (Sigma-Aldrich) were then added, and data were acquired on the FACS Calibur (BD Biosciences). The cell cycle analysis was carried out using ModFIT software (BD Biosciences).

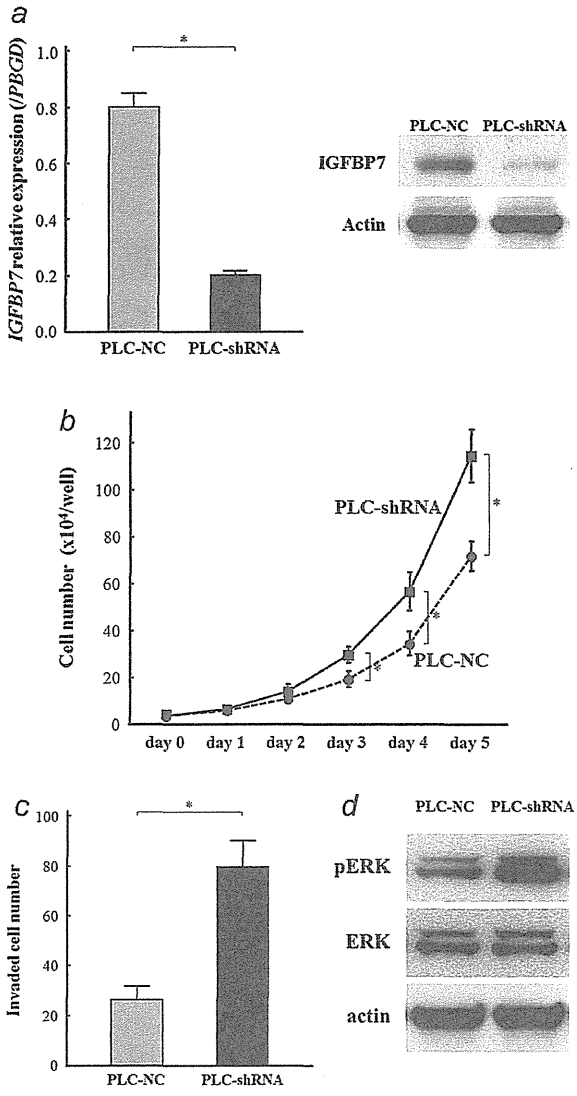

Figure 1. Characteristics of PLC/PRF/5 transfected with shRNA against *IGFBP7*. (*a*) qRT-PCR (Left panel) and western blot analysis (Right panel) indicated a significant decrease in IGFBP7 in cells transfected with shRNA compared to control cells (*$p < 0.05$). (*b*) Proliferation assays showed significantly quicker growth in the IGFBP7-suppressed cells compared with the control cells (*$p < 0.05$). (*c*) The invasion assay showed that the invasive ability of the IGFBP7-suppressed cells was significantly greater than that of the control cells (*$p < 0.05$). (*d*) Western blot analysis demonstrated significantly increased pERK expression in the IGFBP7-supperessed cells compared to the control cells. Data are mean ± SD of 3 experiments.

Immunohistochemical staining

Resected tissue samples were fixed in 10% buffered formalin and finally embedded in paraffin. Immunohistochemical staining for IGFBP7 in the same samples was performed as described previously.[17,20] Briefly, after deparaffinization and blocking, the sections were incubated overnight at 4°C with polyclonal goat anti-human IGFBP7 antibody, and then counterstained with Mayer's hematoxylin. IGFBP7 expression was defined as the presence of specific staining in the cytoplasm of cancer cells. IGFBP7 expression was evaluated as positive or negative, as previously prescribed.[17]

Statistical analysis

Data are expressed as mean ± SD. Differences between groups were assessed using the χ^2-test, and continuous variables were compared using Student's *t*-test. Survival rates were calculated according to the Kaplan-Meier method and compared using the log-rank test. Statistical analysis was performed using StatView (version 5.0; SAS Institute, Cary, NC). A p value < 0.05 was considered statistically significant.

Results

In vitro studies

IGFBP7 downregulation promotes proliferation and invasive activity. First, *IGFBP7* expression was examined by qRT-PCR in 4 HCC cell lines, PLC/PRF/5, HuH7, HLE and HepG2. The *IGFBP7* expression levels in PLC/PRF/5 and HuH7 were the highest and lowest of the 4 cell lines, respectively. A plasmid coding for shRNA against *IGFBP7* was then transfected into PLC/PRF/5, whose IGFBP7 expression level was the highest in the 4 cell lines. The IGFBP7 expression was suppressed by the transfection, as confirmed by qRT-PCR and western blot analysis (Fig. 1*a*). The proliferation assay showed significantly more rapid growth in the IGFBP7-suppressed cells compared to control cells (Fig. 1*b*). In addition, the invasive ability of the IGFBP7-suppressed cells was significantly greater than that of the control cells (Fig. 1*c*). Based on previous studies that IGFBP7 downregulation promotes cell proliferation through ERK signaling, we analyzed the levels of total ERK and pERK in our cells.[10,21] pERK expression was significantly increased in the IGFBP7-supperessed cells, while total ERK expression was not changed, which coincided with previous reports (Fig. 1*d*). On the other hand, as we previously reported, there were no significant differences in the expression of total Akt or phoshorylated Akt between the IGFBP7-supperessed cells and the control cells.[17]

Downregulation of IGFBP7 attenuates apoptosis. The extent of apoptosis of these cells was examined by the Annexin V assay. The percentages of early apoptotic cells and late apoptotic cells defined by Annexin V-positive/PI-negative cells and Annexin V-positive/PI-positive cells respectively were significantly lower in the IGFBP7-suppressed cells than those in the control cells (Fig. 2*a*).[22] This significant difference of the extent of apoptosis was also confirmed under the condition where apoptosis is induced by some agents, which was reported previously.[17] Next, the expression of proteins related to apoptosis was examined. The result showed that cleaved caspase-3 and cleaved PARP are significantly decreased in

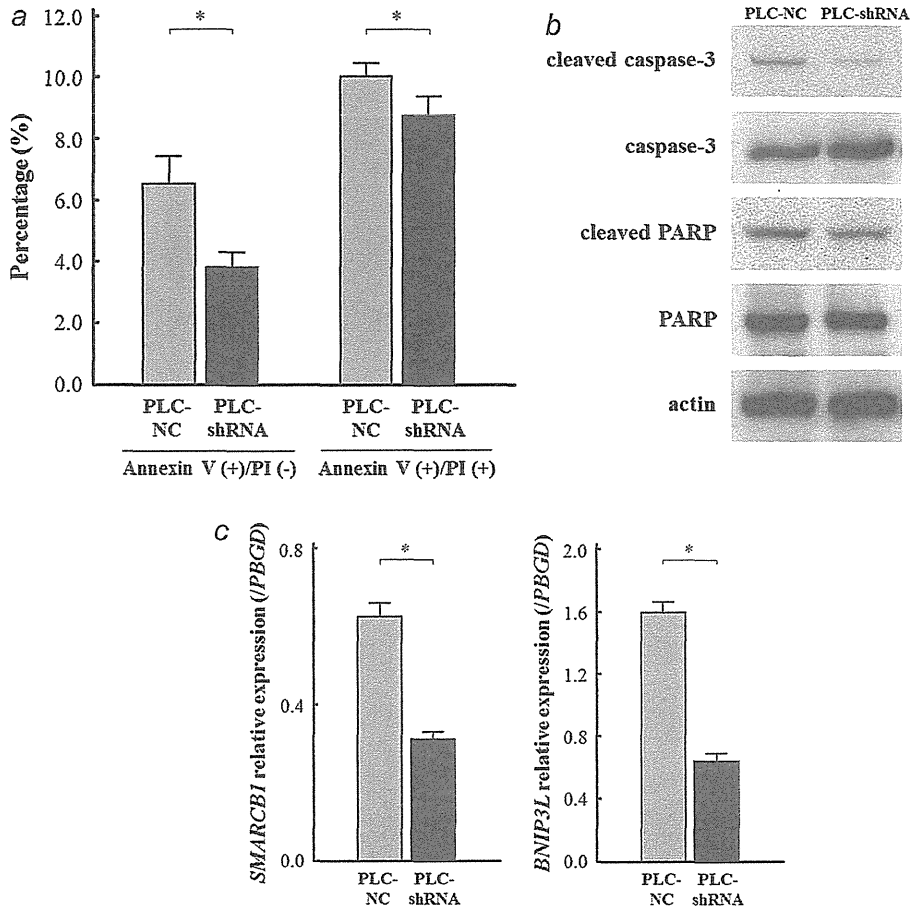

Figure 2. The extent of apoptosis evaluated by the amount of apoptotic cells and the expression of apoptosis-related molecules. (*a*) The Annexin V assay showed the percentage of cells in early apoptosis and in late apoptosis defined by Annexin V-positive/PI-negative cells and Annexin V-positive/PI-positive cells respectively were significantly lower in the IGFBP7-suppressed cells than the control cells (*$p < 0.05$). (*b*) Cleaved caspase-3 and cleaved PARP were decreased in the IGFBP7-suppressed cells. (*c*) qRT-PCR indicated that *SMARCB1* (Left panel) and *BNIP3L* (Right panel) expression levels were significantly decreased in the IGFBP7-supressed cells than the control cells (*$p < 0.05$). Data are mean ± SD of 3 experiments.

the IGFBP7-suppressed cells, while total caspase-3 and PARP expressions were not changed (Fig. 2*b*). In addition, since apoptosis induced by IGFBP7 was reported to occur *via* SMARCB1 and BNIP3L upregulation, we also evaluated the expression levels of *SMARCB1* and *BNIP3L* by qRT-PCR.[10] The results showed that *SMARCB1* and *BNIP3L* expressions were significantly decreased in the IGFBP7-supressed cells compared with the control cells (Fig. 2*c*).

Downregulation of IGFBP7 promotes cell cycle progression. The influence of IGFBP7 on cell cycle was examined by flow cytometric analysis. Prior to the examination, cells were synchronized in the G_0/G_1 phase by serum starvation for 72 hr, and then put back in the regular medium with 10% fetal bovine serum. Dynamic changes in percentage between G_0/G_1 phase and S phase are shown in Figure 3*a*. The proportion of G_0/G_1 phase and S phase on the end of the starvation (0 hr) was almost comparable between the IGFBP7-suppressed cells and the control cells. As shown in Figure 4, the time with minimum percentage of G_0/G_1 phase and maximum percentage of S phase was 24 hr in the control cells, while the time was 12 hr in the IGFBP7-suppressed cells, which suggests that the cell cycle progression was more rapid in the IGFBP7-suppressed cells than that in the control cells. Furthermore, we found that cyclin D1 and cyclin E were increased and p27 was decreased in the IGFBP7-suppressed cells than those in the control cells, and that there was no significant difference in p21 expression between the 2 cells, which was agreement with more rapid cell cycle progression in the IGFBP7-suppressed cells (Fig. 3*b*).

Transfection of IGFBP7 attenuates proliferation and invasive activity. Next, the *IGFBP7* expression plasmid was transfected into HuH7, whose IGFBP7 expression level was the lowest in the 4 HCC cell lines. The IGFBP7 expression was increased by

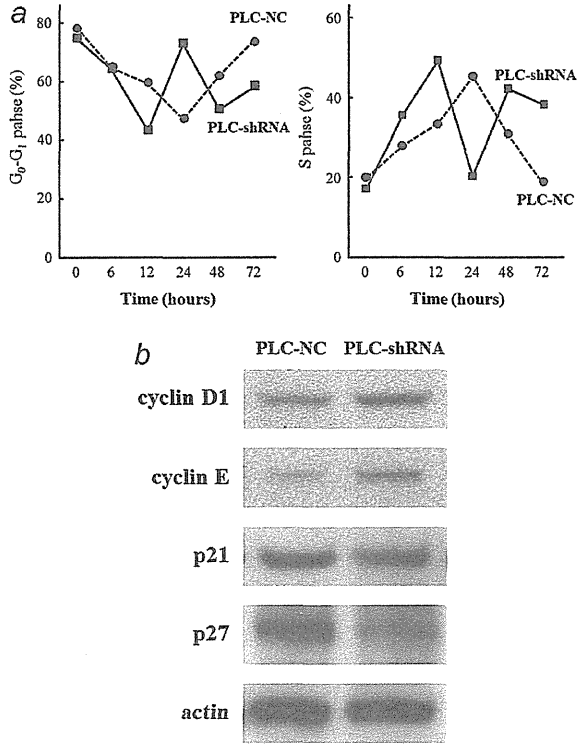

Figure 3. Cell cycle progression assessed by a flow cytometric analysis and the expression of cell cycle-related molecules. (*a*) Time with minimum percentage of G_0/G_1 phase (Left panel) and maximum percentage of S phase (Right panel) was 24 hr and 12 hr in the control cells and the IGFBP7-suppressed cells, respectively. (*b*) Cyclin D1 and cyclin E were increased and p27 was decreased in the IGFBP7-suppressed cells than the control cells, and there was no significant difference in p21 expression between the 2 cells.

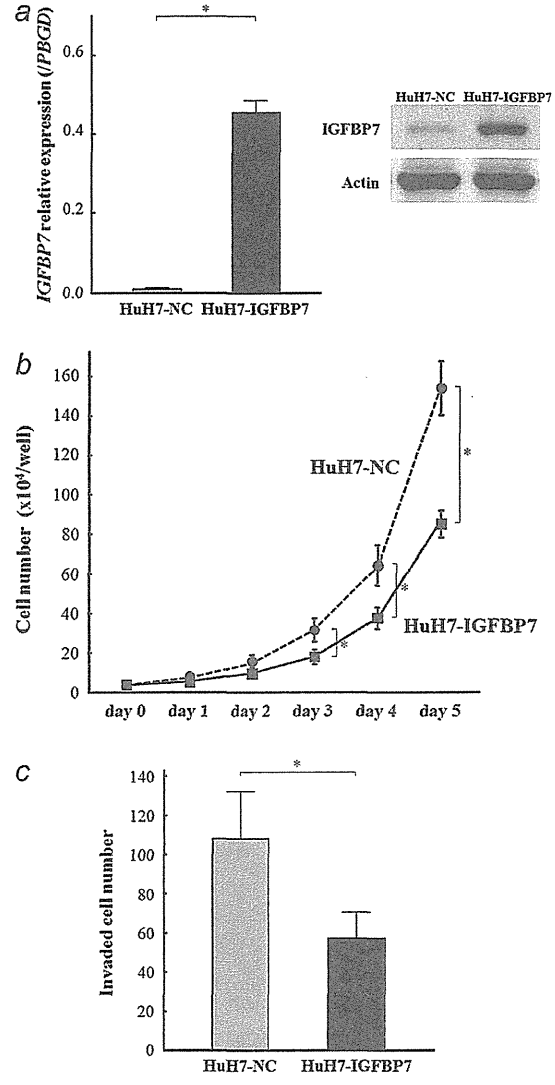

Figure 4. Characteristics of HuH7 transfected with *IGFBP7* expression plasmid. (*a*) qRT-PCR (Left panel) and western blot analysis (Right panel) indicated a significant increase in IGFBP7 in cells transfected with *IGFBP7* expression plasmid compared with control cells (*$p < 0.05$). (*b*) Proliferation assays showed significantly slower growth in the IGFBP7-overexpressing cells compared to the control cells (*$p < 0.05$). (*c*) The invasion assay showed that the invasive ability of the IGFBP7-overexpressing cells was significantly weaker than that of the control cells (*$p < 0.05$). Data are mean ± SD of 3 experiments.

the transfection, as confirmed by qRT-PCR and western blot analysis (Fig. 4*a*). The proliferation assay showed significantly less rapid growth in the IGFBP7-overexpressing cells compared to the control cells (Fig. 4*b*). In addition, the invasive ability of the IGFBP7-overexpressing cells was significantly weaker than that of the control cells (Fig. 4*c*), which were consistent to the results of the above shRNA plasmid experiments.

In vivo studies

IGFBP7 expression correlates with tumor-related factors in clinical HCC samples.. Next, IGFBP7 expression in the tumoral leison was evaluated in clinical sample by immunohistochemical staining. The immunohistochemical analysis showed that among the 104 patients examined, 67 patients (64.4%) showed positive staining for IGFBP7 and the remaining 37 patients (35.6%) were negative for IGFBP7. The immunohistochemical findings of representative cases are shown in Figure 5*a*. The clinicopathological factors related to IGFBP7 expression status of the 104 patients are summarized in Table 1. The data indicated that IGFBP7 expression was significantly associated with maximum tumor size and vascular invasion ($p < 0.0001$, $p = 0.0095$, respectively).

On the other hand, the IGFBP7 expression in nontumoral lesion was homogenously observed in the cytoplasm of cells in all the 104 patients. The immunohistochemically

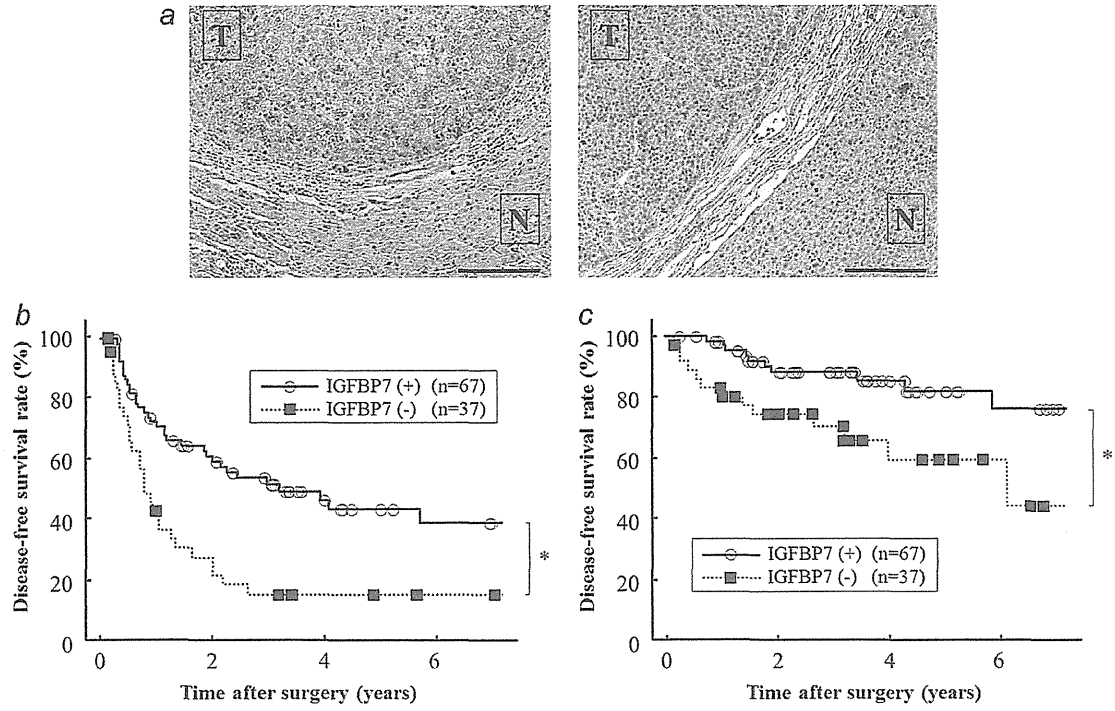

Figure 5. IGFBP7 expression and postoperative outcome in HCC patients. (*a*) Immunohistochemical findings in representative positive case (Left panel) and negative case (Right panel). T, tumoral lesion; N, non-tumoral lesion. Bar = 200 μm. Disease-free survival (*b*) and overall survival (*c*) in patients negative for IGFBP7 expression were significantly poorer than in cells expressing IGFBP7 (*$p < 0.05$).

Table 1. Clinicopathological characteristics of patients with HCC according to IGFBP7 status

	IFGFBP7 (+) (n = 67)	IGFBP7 (−) (n = 37)	p-value
Clinical factors			
Gender (male/female)	53/14	29/8	0.9308
Age (years)[1]	65 ± 10	63 ± 10	0.3900
HBs-Ag (−/+)	52/15	30/7	0.6783
Anti-HCV Ab (−/+)	29/38	15/22	0.7863
Child-Pugh classification (A/B)	58/9	29/8	0.2796
Liver cirrhosis (−/+)	31/36	20/17	0.4470
Tumor-related factors			
AFP (ng/ml)[1]	15,155 ± 122,143	30,243 ± 86,058	0.5075
PIVKA-II (mAU/ml)[1]	26,656 ± 87,446	151,639 ± 1,221,431	0.5365
Number of tumors (single/multiple)	47/20	21/16	0.1693
Maximum tumor size (cm)	3.2 ± 1.7	6.5 ± 4.7	<0.0001
Vascular invasion (−/+)	58/9	24/13	0.0095
Edmondson-Steiner grade (I,II/III,IV)	31/36	11/26	0.0998

[1]Data are expressed as mean ± SD.
Abbreviations: IGFBP7, insulin-like growth factor binding protein 7; HBs-Ag, hepatitis B surface antigen; Anti-HCV Ab, anti-hepatic C virus antibody; AFP:, alpha-fetoprotein; PIVKA-II, protein induced by vitamin K absence or antagonists-II.

determined IGFBP7 expression level was similar between 53 cirrhotic patients and the remaining 51 non-cirrhotic patients.

IGFBP7 downregulation is an independent significant predictor for postoperative outcome in HCC patients. The disease-free survival (DFS) in patients without IGFBP7 expression (1-/

Table 2. Statistical analysis of disease-free survival and overall survival of patients with HCC

	Disease-free survival				Overall survival			
	Univariate	Multivariate			Univariate	Multivariate		
	p-value	OR	95% CI	*p*-value	*p*-value	OR	95% CI	*p*-value
Clinical factors								
Gender (male/female)	0.2192				0.1968			
Age (years) (≤64/>64)	0.5542				0.8018			
HBs-Ag (−/+)	0.2440				0.3605			
Anti-HCV Ab (−/+)	0.9405				0.5034			
Child-Pugh classification (A/B)	0.2586				0.7501			
Liver cirrhosis (−/+)	0.1429				0.5587			
Tumor-related factors								
AFP (ng/ml) (≤400/>400)	0.0629				0.1042			
PIVKA-II (mAU/ml) (≤40/>40)	0.2912				0.1563			
Number of tumors (single/multiple)	0.0025	1.659	0.978–2.815	0.0604	0.0007	2.288	0.905–5.780	0.0801
Maximum tumor size (cm) (≤5/>5)	0.0001	1.387	0.737–2.611	0.3100	0.0290	1.512	0.579–3.949	0.3991
Vascular invasion (−/+)	<0.0001	2.681	1.400–5.135	0.0029	<0.0001	4.649	1.705–12.679	0.0027
Edmondson-Steiner grade (I,II/III,IV)	0.0392	1.520	0.894–2.574	0.1225	0.0180	5.587	1.616–19.231	0.0066
IGFBP7 status (−/+)	0.0007	1.919	1.112–3.313	0.0192	0.0063	2.659	1.102–6.418	0.0296

Abbreviations: IGFBP7, insulin-like growth factor binding protein 7; HBs-Ag, hepatitis B surface antigen; Anti-HCV Ab, anti-hepatic C virus antibody; AFP:, alpha-fetoprotein; PIVKA-II, protein induced by vitamin K absence or antagonists-II; OR, odds ratio; 95% CI, 95% confidence interval.

3-/5-year: 42.9%/15.3%/15.3%) was significantly poorer than that in patients showing IGFBP7 expression (1-/3-/5-year: 70.9%/51.8%/43.6%) ($p = 0.0002$; Fig. 5*b*). Univariate analyses showed that number of tumors ($p = 0.0025$), maximum tumor size ($p = 0.0001$), presence/absence of vascular invasion ($p < 0.0001$), and Edmondson-Steiner grade ($p = 0.0392$) all significantly correlated with DFS, in addition to IGFBP7 status (Table 2). Multivariate analysis for DFS using the above 5 factors identified presence/absence of vascular invasion and IGFBP7 status as independent significant factors (Table 2).

The overall survival (OS) rate in patients without IGFBP7 expression (1-/3-/5-year: 83.4%/70.2%/59.2%) was also significantly lower than that in patients with positive IGFBP7 expression (1-/3-/5-year: 98.5%/88.4%/82.0%) ($p = 0.0063$; Fig. 5*c*). By univariate analysis, number of tumors ($p = 0.0007$), maximum tumor size ($p = 0.0290$), presence/absence of vascular invasion ($p < 0.0001$), and Edmondson-Steiner grade ($p = 0.0180$) were also significantly correlated with OS (Table 2). Multivariate analysis using the above 5 factors identified presence/absence of vascular invasion, Edmondson-Steiner grade, and IGFBP7 status as independent significant factors in OS (Table 2). Thus, IGFBP7 expression was an overall independent significant factor for postoperative prognosis in HCC patients.

Discussion

In this study, we first analyzed IGFBP7 function *in vitro* experiments. The results demonstrated that IGFBP7 downregulation was significantly associated with rapid growth and proliferation of HCC cells. In addition, the cells showed decreased apoptotic cell numbers and expression of apoptosis-related proteins, enhancement of ERK signaling, and rapid cell cycle progression. Considering the implicated tumor suppression activity of IGFBP7, the results of this study are consistent with previous similar reports.[7,9–11,14,15,21] We also previously reported a significant association of IGFBP7 downregulation with resistance to some chemotherapeutic drugs in HCC cells.[17] Taken together, it seems apparent that IGFBP7 downregulation is significantly associated with the malignant potential of cancer cells including proliferation, invasiveness, and resistance to chemotherapeutic drugs. To our knowledge, this is the first study to examine the functional role of IGFBP7 in HCC. On the other hand, the cause-and-effect relationship between the IGFBP7 downregulation and the malignant potential is still unsolved, which is expected to be elucidated by further studies in future.

This study also assessed the prognostic significance of IGFBP7 expression in resected human HCC samples. From these findings, IGFBP7 downregulation was significantly associated with tumor progression and postoperative poor prognosis in our patients group, and IGFBP7 status was identified as an independent significant prognostic factor, in addition to other well-known factors. This finding was consistent with the results of the *in vitro* experiments and serves to suggest that assessing the IGFBP7 expression status of patients with HCC could improve the prediction of prognosis.

We have reported some studies of significant prognostic predictors after surgery for HCC.[20,23–38] In one of the studies, based on cDNA microarray analysis, we identified a set of multiple genes whose expressions were significantly different

between patients with good prognosis and those with poor prognosis, and revealed that the gene set was one of the independent prognostic factors.[38] IGFBP7 was not included in the gene set because the difference of the expression level was not large between the 2 groups, but the IGFBP7 expression level examined by the microarray analysis was also significantly correlated to the prognosis. This result seems to be consistent with the result of this study. In addition, considering the significant inverse correlation of IGFBP7 expression to the extent of apoptosis and cell cycle progression confirmed by the *in vitro* experiments, our previous reports of apoptosis- and cell cycle-related molecules as prognostic factors are in agreement with the prognostic impact of IGFBP7.[25,26,34,35] Furthermore, we have reported that angiogenesis-related molecules such as angiopoietin-2 and hypoxia-induced factor-1α are significant factors for postoperative prognosis.[33] Considering that IGFBP7 was reported to block angiogenesis in human vascular endothelial cells, it may be possible that there is a significant correlation between IGFBP7 expression and the angiogenesis-related molecules, though we did not examine it in this study.[39]

IGFBP7 is a secreted protein, and recombinant IGFBP7 is commonly purified.[40,41] Indeed, previous studies of IGFBP7 function have expressed the protein exogenously using IGFBP7 viral vectors or by administering recombinant protein.[39] In addition, IGFBP7 has also been studied as a possible therapeutic agent for treatment of malignancies that are dependent on BRAF-MEK-ERK signaling.[10,42] Thus, recombinant IGFBP7 could be potentially suitable therapeutically to improve the poor prognosis of HCC patients lacking IGFBP7 expression. In addition, IGFBP7 expression is also subject to epigenetic modification, and aberrant methylation of CpG islands in the *IGFBP7* promoter region was confirmed in several kinds of cancers.[10,43] In this regard, Wajapeyee *et al.*[10] showed that treatment of melanoma cell lines with DNA methyltransferase inhibitor, 5-aza-2′-deoxycytidine, restored IGFBP7 expression. Such a finding suggests a therapeutic application whereby IGFBP7 expression and thus function are restored using a DNA methyltransferase inhibitor. Exploring these therapeutic interventions against HCC was unfortunately beyond the scope of this study, and further studies are definitely needed in this regard.

In summary, we found that IGFBP7 downregulation was significantly associated with both tumor progression and clinical outcome in HCC. This result suggested that analysis of IGFBP7 expression in patients might help to predict prognosis, and that IGFBP7 could be a novel therapeutic target in HCC patients with poor prognosis.

References

1. Block TM, Mehta AS, Fimmel CJ, Jordan R. Molecular viral oncology of hepatocellular carcinoma. *Oncogene* 2003; 22:5093–107.
2. Bosch FX, Ribes J, Diaz M, Cleries R. Primary liver cancer: worldwide incidence and trends. *Gastroenterology* 2004;127: S5–S16.
3. Zhu AX. Systemic therapy of advanced hepatocellular carcinoma: how hopeful should we be? *Oncologist* 2006;11:790–800.
4. Tung-Ping Poon R, Fan ST, Wong J. Risk factors, prevention, and management of postoperative recurrence after resection of hepatocellular carcinoma. *Ann Surg* 2000; 232:10–24.
5. Zhao WH, Ma ZM, Zhou XR, Feng YZ, Fang BS. Prediction of recurrence and prognosis in patients with hepatocellular carcinoma after resection by use of CLIP score. *World J Gastroenterol* 2002;8:237–42.
6. Zhou J, Tang ZY, Wu ZQ, Zhou XD, Ma ZC, Tan CJ, Shi YH, Yu Y, Qiu SJ, Fan J. Factors influencing survival in hepatocellular carcinoma patients with macroscopic portal vein tumor thrombosis after surgery, with special reference to time dependency: a single-center experience of 381 cases. *Hepatogastroenterology* 2006;53: 275–80.
7. Mutaguchi K, Yasumoto H, Mita K, Matsubara A, Shiina H, Igawa M, Dahiya R, Usui T. Restoration of insulin-like growth factor binding protein-related protein 1 has a tumor-suppressive activity through induction of apoptosis in human prostate cancer. *Cancer Res* 2003;63: 7717–23.
8. Sato Y, Chen Z, Miyazaki K. Strong suppression of tumor growth by insulin-like growth factor-binding protein-related protein 1/tumor-derived cell adhesion factor/mac25. *Cancer Sci* 2007;98:1055–63.
9. Kato MV. A secreted tumor-suppressor, mac25, with activin-binding activity. *Mol Med* 2000;6:126–35.
10. Wajapeyee N, Serra RW, Zhu X, Mahalingam M, Green MR. Oncogenic BRAF induces senescence and apoptosis through pathways mediated by the secreted protein IGFBP7. *Cell* 2008;132:363–74.
11. Wilson HM, Birnbaum RS, Poot M, Quinn LS, Swisshelm K. Insulin-like growth factor binding protein-related protein 1 inhibits proliferation of MCF-7 breast cancer cells via a senescence-like mechanism. *Cell Growth Differ* 2002;13:205–13.
12. Lin J, Lai M, Huang Q, Ruan W, Ma Y, Cui J. Reactivation of IGFBP7 by DNA demethylation inhibits human colon cancer cell growth in vitro. *Cancer Biol Ther* 2008; 7:1896–900.
13. Burger AM, Zhang X, Li H, Ostrowski JL, Beatty B, Venanzoni M, Papas T, Seth A. Down-regulation of T1A12/mac25, a novel insulin-like growth factor binding protein related gene, is associated with disease progression in breast carcinomas. *Oncogene* 1998;16:2459–67.
14. Landberg G, Ostlund H, Nielsen NH, Roos G, Emdin S, Burger AM, Seth A. Downregulation of the potential suppressor gene IGFBP-rP1 in human breast cancer is associated with inactivation of the retinoblastoma protein, cyclin E overexpression and increased proliferation in estrogen receptor negative tumors. *Oncogene* 2001;20:3497–505.
15. Ruan WJ, Lin J, Xu EP, Xu FY, Ma Y, Deng H, Huang Q, Lv BJ, Hu H, Cui J, Di MJ, Dong JK, et al. IGFBP7 plays a potential tumor suppressor role against colorectal carcinogenesis with its expression associated with DNA hypomethylation of exon 1. *J Zhejiang Univ Sci B* 2006;7:929–32.
16. Kondo M, Nagano H, Wada H, Damdinsuren B, Yamamoto H, Hiraoka N, Eguchi H, Miyamoto A, Yamamoto T, Ota H, Nakamura M, Marubashi S, et al. Combination of IFN-alpha and 5-fluorouracil induces apoptosis through IFN-alpha/beta receptor in human hepatocellular carcinoma cells. *Clin Cancer Res* 2005;11:1277–86.
17. Tomimaru Y, Eguchi H, Wada H, Noda T, Murakami M, Kobayashi S, Marubashi S, Takeda Y, Tanemura M, Umeshita K, Doki Y, Mori M, et al. Insulin-like growth

factor-binding protein 7 alters the sensitivity to interferon-based anticancer therapy in hepatocellular carcinoma cells. *Br J Cancer* 2010;102:1483–90.
18. Nakamura M, Nagano H, Sakon M, Yamamoto T, Ota H, Wada H, Damdinsuren B, Noda T, Marubashi S, Miyamoto A, Takeda Y, Umeshita K, et al. Role of the Fas/FasL pathway in combination therapy with interferon-alpha and fluorouracil against hepatocellular carcinoma in vitro. *J Hepatol* 2007;46:77–88.
19. Eguchi H, Nagano H, Yamamoto H, Miyamoto A, Kondo M, Dono K, Nakamori S, Umeshita K, Sakon M, Monden M. Augmentation of antitumor activity of 5-fluorouracil by interferon alpha is associated with up-regulation of p27Kip1 in human hepatocellular carcinoma cells. *Clin Cancer Res* 2000;6: 2881–90.
20. Kondo M, Yamamoto H, Nagano H, Okami J, Ito Y, Shimizu J, Eguchi H, Miyamoto A, Dono K, Umeshita K, Matsuura N, Wakasa K, et al. Increased expression of COX-2 in nontumor liver tissue is associated with shorter disease-free survival in patients with hepatocellular carcinoma. *Clin Cancer Res* 1999;5:4005–12.
21. Vizioli MG, Sensi M, Miranda C, Cleris L, Formelli F, Anania MC, Pierotti MA, Greco A. IGFBP7: an oncosuppressor gene in thyroid carcinogenesis. *Oncogene* 2010; 29:3835–44.
22. Lugli E, Troiano L, Ferraresi R, Roat E, Prada N, Nasi M, Pinti M, Cooper EL, Cossarizza A. Characterization of cells with different mitochondrial membrane potential during apoptosis. *Cytometry A* 2005;68:28–35.
23. Arai I, Nagano H, Kondo M, Yamamoto H, Hiraoka N, Sugita Y, Ota H, Yoshioka S, Nakamura M, Wada H, Damdinsuren B, Kato H, et al. Overexpression of MT3-MMP in hepatocellular carcinoma correlates with capsular invasion. *Hepatogastroenterology* 2007;54:167–71.
24. Damdinsuren B, Nagano H, Kondo M, Yamamoto H, Hiraoka N, Yamamoto T, Marubashi S, Miyamoto A, Umeshita K, Dono K, Nakamori S, Wakasa K, et al. Expression of Id proteins in human hepatocellular carcinoma: relevance to tumor dedifferentiation. *Int J Oncol* 2005; 26:319–27.
25. Ito Y, Matsuura N, Sakon M, Miyoshi E, Noda K, Takeda T, Umeshita K, Nagano H, Nakamori S, Dono K, Tsujimoto M, Nakahara M, et al. Expression and prognostic roles of the G1-S modulators in hepatocellular carcinoma: p27 independently predicts the recurrence. *Hepatology* 1999;30:90–9.
26. Ito Y, Matsuura N, Sakon M, Takeda T, Umeshita K, Nagano H, Nakamori S, Dono K, Tsujimoto M, Nakahara M, Nakao K, Monden M. Both cell proliferation and apoptosis significantly predict shortened disease-free survival in hepatocellular carcinoma. *Br J Cancer* 1999;81:747–51.
27. Kittaka N, Takemasa I, Seno S, Takeda Y, Kobayashi S, Marubashi S, Dono K, Umeshita K, Nagano H, Matsuda H, Monden M, Mori M, et al. Exploration of potential genomic portraits associated with intrahepatic recurrence in human hepatocellular carcinoma. *Ann Surg Oncol* 2010;17:3145–54.
28. Kittaka N, Takemasa I, Takeda Y, Marubashi S, Nagano H, Umeshita K, Dono K, Matsubara K, Matsuura N, Monden M. Molecular mapping of human hepatocellular carcinoma provides deeper biological insight from genomic data. *Eur J Cancer* 2008;44:885–97.
29. Miyamoto A, Nagano H, Sakon M, Fujiwara Y, Sugita Y, Eguchi H, Kondo M, Arai I, Morimoto O, Dono K, Umeshita K, Nakamori S, et al. Clinical application of quantitative analysis for detection of hematogenous spread of hepatocellular carcinoma by real-time PCR. *Int J Oncol* 2001;18:527–32.
30. Morimoto O, Nagano H, Sakon M, Fujiwara Y, Yamada T, Nakagawa H, Miyamoto A, Kondo M, Arai I, Yamamoto T, Ota H, Dono K, et al. Diagnosis of intrahepatic metastasis and multicentric carcinogenesis by microsatellite loss of heterozygosity in patients with multiple and recurrent hepatocellular carcinomas. *J Hepatol* 2003;39:215–21.
31. Noda T, Nagano H, Tomimaru Y, Murakami M, Wada H, Kobayashi S, Marubashi S, Eguchi H, Takeda Y, Tanemura M, Umeshita K, Kim T, et al. Prognosis of hepatocellular carcinoma with biliary tumor thrombi following liver surgery. *Surgery* 2011;149:371–7.
32. Sakon M, Umeshita K, Nagano H, Eguchi H, Kishimoto S, Miyamoto A, Ohshima S, Dono K, Nakamori S, Gotoh M, Monden M. Clinical significance of hepatic resection in hepatocellular carcinoma: analysis by disease-free survival curves. *Arch Surg* 2000;135:1456–9.
33. Wada H, Nagano H, Yamamoto H, Yang Y, Kondo M, Ota H, Nakamura M, Yoshioka S, Kato H, Damdinsuren B, Tang D, Marubashi S, et al. Expression pattern of angiogenic factors and prognosis after hepatic resection in hepatocellular carcinoma: importance of angiopoietin-2 and hypoxia-induced factor-1 alpha. *Liver Int* 2006;26:414–23.
34. Xu X, Yamamoto H, Sakon M, Yasui M, Ngan CY, Fukunaga H, Morita T, Ogawa M, Nagano H, Nakamori S, Sekimoto M, Matsuura N, et al. Overexpression of CDC25A phosphatase is associated with hypergrowth activity and poor prognosis of human hepatocellular carcinomas. *Clin Cancer Res* 2003;9:1764–72.
35. Xu X, Sakon M, Nagano H, Hiraoka N, Yamamoto H, Hayashi N, Dono K, Nakamori S, Umeshita K, Ito Y, Matsuura N, Monden M. Akt2 expression correlates with prognosis of human hepatocellular carcinoma. *Oncol Rep* 2004; 11:25–32.
36. Yamamoto S, Tomita Y, Nakamori S, Hoshida Y, Nagano H, Dono K, Umeshita K, Sakon M, Monden M, Aozasa K. Elevated expression of valosin-containing protein (p97) in hepatocellular carcinoma is correlated with increased incidence of tumor recurrence. *J Clin Oncol* 2003;21: 447–52.
37. Yang Y, Nagano H, Ota H, Morimoto O, Nakamura M, Wada H, Noda T, Damdinsuren B, Marubashi S, Miyamoto A, Takeda Y, Dono K, et al. Patterns and clinicopathologic features of extrahepatic recurrence of hepatocellular carcinoma after curative resection. *Surgery* 2007;141: 196–202.
38. Yoshioka S, Takemasa I, Nagano H, Kittaka N, Noda T, Wada H, Kobayashi S, Marubashi S, Takeda Y, Umeshita K, Dono K, Matsubara K, et al. Molecular prediction of early recurrence after resection of hepatocellular carcinoma. *Eur J Cancer* 2009;45:881–9.
39. Tamura K, Hashimoto K, Suzuki K, Yoshie M, Kutsukake M, Sakurai T. Insulin-like growth factor binding protein-7 (IGFBP7) blocks vascular endothelial cell growth factor (VEGF)-induced angiogenesis in human vascular endothelial cells. *Eur J Pharmacol* 2009;610:61–7.
40. Akaogi K, Okabe Y, Sato J, Nagashima Y, Yasumitsu H, Sugahara K, Miyazaki K. Specific accumulation of tumor-derived adhesion factor in tumor blood vessels and in capillary tube-like structures of cultured vascular endothelial cells. *Proc Natl Acad Sci USA* 1996;93:8384–9.
41. Oh Y, Nagalla SR, Yamanaka Y, Kim HS, Wilson E, Rosenfeld RG. Synthesis and characterization of insulin-like growth factor-binding protein (IGFBP)-7. Recombinant human mac25 protein specifically binds. IGF-I and -II. *J Biol Chem* 1996;271:30322–5.
42. Wajapeyee N, Kapoor V, Mahalingam M, Green MR. Efficacy of IGFBP7 for treatment of metastatic melanoma and other cancers in mouse models and human cell lines. *Mol Cancer Ther* 2009;8:3009–14.
43. Lin J, Lai M, Huang Q, Ma Y, Cui J, Ruan W. Methylation patterns of IGFBP7 in colon cancer cell lines are associated with levels of gene expression. *J Pathol* 2007; 212:83–90.

Distinct expression of C4.4A in colorectal cancer detected by different antibodies

HIROFUMI YAMAMOTO, RYOTA OSHIRO, MASAHISA OHTSUKA, MAMORU UEMURA, NAOTSUGU HARAGUCHI, JUNICHI NISHIMURA, ICHIRO TAKEMASA, TSUNEKAZU MIZUSHIMA, YUICHIRO DOKI and MASAKI MORI

Department of Surgery, Gastroenterological Surgery, Graduate School of Medicine, Osaka University, Suita, Osaka, Japan

Received July 20, 2012; Accepted September 3, 2012

DOI: 10.3892/ijo.2012.1714

Abstract. The metastasis-associated gene C4.4A encodes a glycolipid-anchored membrane protein expressed in several human malignancies. The present study aimed to perform a detailed assessment of C4.4A expression in colorectal cancer tissues, in terms of intra-cellular localization, intra-tumoral location and difference in molecular weight. To advance this goal, we developed three new antibodies against the C4.4A protein (two polyclonal Abs: C4.4A-119 and C4.4A-277 and one monoclonal Ab: C4.4A GPI-M) to use in addition to the two previously produced polyclonal Abs (C4.4A-81, C4.4A GPI-P). Antibody specificities were confirmed by absorption tests. Western blot analysis and immunohistochemistry showed that the C4.4A-119 and C4.4-277 Abs detected 70-kDa C4.4A, mainly in the cytoplasm, irrespective of intra-tumoral location. The C4.4A GPI-P and C4.4A GPI-M Abs reacted with the membranous ~40-kDa C4.4A, exclusively at the tumor invasive front, and each detected an identical tumor cell population. The tested antibodies showed varied C4.4A detection rates in 33 CRC tissues. The C4.4A-277 Ab yielded the highest positive rate in 29 of 33 CRC tissues (87.9%), while the C4.4A GPI-P and C4.4A GPI-M Abs each only showed 33.3% positivity. The present findings suggest that the GPI anchor signaling sequence may be essential for detecting membranous C4.4A at the invasive front of CRC tissues.

Introduction

The C4.4A protein was first identified in a highly metastatic rat pancreatic adenocarcinoma cell line (1,2). The human homologue of rat C4.4A is located on chromosome 19q13.1-q13.2 and was cloned in 2001 (3). Studies of the molecular structure indicate that C4.4A is a glycosylphosphatidyl-inositol (GPI)-anchored membrane protein with 30% homology to the urokinase-type plasminogen activator receptor (4,5). In normal human tissues, C4.4A mRNA is present in placental tissue, skin, esophagus, and leukocytes (3); but the physiological function of the C4.4A protein is largely unknown. C4.4A expression is upregulated in some types of human malignancies, and human C4.4A mRNA has been detected in cancer cell lines, including melanoma, breast, bladder, and renal cell carcinoma, as well as in tumor tissue samples from malignant melanoma, colorectal cancer (CRC), breast cancer, lung carcinoma, and urothelial tumors (5-10).

We previously detected C4.4A protein expression on the plasma membranes of tumor cells at the invasive front in 25.6% of 132 CRCs (11). In that study, we used a polyclonal antibody that recognizes the C4.4A C-terminus containing the GPI anchor signaling sequence. In contrast, Paret *et al* (9) reported that 85.4% of CRC tissues showed distinct C4.4A expression by immunohistochemistry, and they did not mention an invasive front-specific expression pattern. We also observed that another C4.4A polyclonal antibody that was raised against amino acids near the N-terminus did not react with the C4.4A protein in CRC tissue samples, while it did recognize C4.4A in the esophageal squamous epithelium (11). These findings suggest that distinct antibodies detect different species of the C4.4A protein.

In the present study, we further investigated C4.4A expression in CRC tissue samples. We developed three novel antibodies (two polyclonal antibodies: C4.4A-119 and C4.4A-277, and one monoclonal antibody: C4.4A GPI-M) and tested them in addition to the two previously produced antibodies (C4.4A-81, and C4.4A GPI-P) (11). Using these antibodies for immunohistochemistry, we performed a detailed assessment of the C4.4A protein with regard to expression rates in CRC cases, intra-cellular localization in tumor cells (cytoplasm or plasma membrane), and intra-tumoral localization (invasive front, or intermediate portion to superficial portion of the cancer body). Western blot analysis was also performed to determine the molecular weight of the C4.4A protein bound by each antibody. Our results show that GPI anchor signaling sequence may be essential for detecting membranous C4.4A at the invasive front of CRC, which is of clinical significance.

Correspondence to: Dr Hirofumi Yamamoto, Department of Surgery, Gastroenterological Surgery, Graduate School of Medicine, Osaka University, 2-2 Yamada-oka, Suita, Osaka 565-0871, Japan
E-mail: hyamamoto@gesurg.med.osaka-u.ac.jp

Abbreviations: Ab, antibody; CRC, colorectal cancer; GPI, glycosyl-phosphatidyl-inositol

Key words: C4.4A, colorectal cancer, GPI anchor, localization

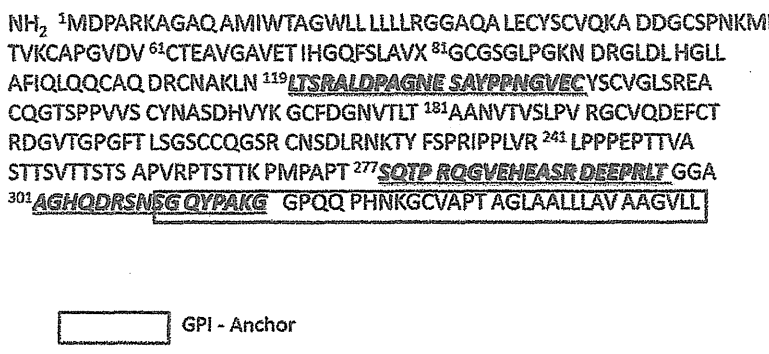

Figure 1. Amino acid sequences of the C4.4A protein with the epitopes employed as immunogens in bold. C4.4A-81 starts at AA 81, C4.4A-119 at AA 119, C4.4A-277 at AA 277, and C4.4A GPI-P and C4.4A GPI-M start at AA 301. The boxed area indicates the GPI anchor signaling sequence. ^{309}SGQYPAKG is destined to be cut off when the C4.4A molecule is anchored onto the plasma membrane.

Materials and methods

Tissue samples and cell lines. All colorectal tissue samples (n=33) were collected during surgery at the Department of Surgery, Osaka University (Osaka, Japan). Samples were fixed in buffered formalin at 4˚C overnight, processed through graded ethanol solutions, and embedded in paraffin. The specimens were appropriately used, with the approval of the Ethics Committee at the Graduate School of Medicine, Osaka University. The human colon cancer cell line HCT116 was obtained from the American Type Culture Collection (Manassas, VA, USA). Cells were grown in DMEM supplemented with 10% fetal bovine serum (FBS), 100 U/ml penicillin, and 100 μg/ml streptomycin, at 37˚C in a humidified incubator, under 5% CO_2 in air.

Antibodies. To generate rabbit polyclonal antibodies, rabbits were immunized with the target peptides bound to thyroglobulin. The C4.4A-specific IgG was purified by passage of the antisera over a peptide column in which the peptide had been coupled to the beads. To generate the anti-human C4.4A monoclonal antibody, mice (BALB/c or BDF1, Charles River, Japan) were immunized weekly with thyroglobulin-conjugated C4.4A peptides (50 μg/mouse). We used partial human C4.4A peptide consisting of amino acid residues 301-316 (AGHQDRSNSGQYPAKG) as an immunogen for the C-terminus containing a portion of the GPI anchor. The cysteine residue was combined in the immunogen beforehand for binding to the carrier protein, bovine thyroglobulin. After four immunizations, the spleen was isolated and fused with X63Ag8 myeloma cells. Through limited dilution and the screening process, the 11A1 clone was selected. The rabbit anti-human actin antibody was purchased from Sigma-Aldrich (St. Louis, MO, USA).

Immunohistochemistry. Tissue sections (4-μm thick) were prepared from paraffin-embedded blocks. After antigen retrieval treatment in 10 mM citrate buffer (pH 6.0) at 95˚C for 40 min, immunostaining was carried out using the Vectastain ABC peroxidase kit (Vector Laboratories, Burlingame, CA, USA) as we have described previously (12,13). The slides were incubated overnight at 4˚C with appropriate antibodies diluted as follows: C4.4A-119, 1:20; C4.4A-278, 1:20; C4.4A GPI-P, 1:200; and C4.4A GPI-M, 1:50. Non-immunized rabbit IgG or mouse IgG (Vector Laboratories) was substituted for the primary antibody as a negative control to exclude possible false-positive responses from the secondary antibody or from non-specific binding of IgG.

Western blot analysis. Western blot analysis was performed as described previously (14,15). Briefly, 20-μg protein samples were separated by 12.5% polyacrylamide gel electrophoresis followed by electroblotting onto a polyvinylidene difluoride membrane (PVDF). The membrane was incubated for 1 h with the primary antibodies at the following concentrations: C4.4A-119, 1:50; C4.4A-278, 1:50; C4.4A GPI-P, 1:500; C4.4A GPI-M, 1:50; and actin, 1:1000. The protein bands were detected using the Amersham Enhanced Chemiluminescence (ECL) Detection System (Amersham Biosciences Corp., NJ, USA).

Absorption test. For absorption testing, an excess amount of immunogen peptide was added to the antibody (20 mol:1 mol), the mixture was incubated overnight at 4˚C and was used instead of the primary antibody.

Results

Generation of C4.4A antibodies. In this study, we generated two novel rabbit anti-human C4.4A polyclonal antibodies, C4.4A-119 and C4.4A-277, and a mouse anti-human C4.4A monoclonal antibody, C4.4A GPI-M. The immunogens used for C4.4A-119 and C4.4A-277 were ^{119}*LTSRALDPAGNE SAYPPNGVEC* and ^{277}*SQTP RQGVEHEASR DEEPRLT*, respectively (Fig. 1). The anti-human C4.4A monoclonal antibody C4.4A GPI-M was raised against ^{301}*AGHQDRSNSGQYPAKG* at the C-terminus containing a portion of the GPI anchor signaling sequence (Fig. 1). The ^{301}*AGHQDRSNSGQYPAKG* immunogen was used in our previous study to generate a GPI-related polyclonal antibody, anti-human C4.4A antibody-2 antibody, which we also used in the present study for comparison (designated as C4.4A GPI-P in this study for simplicity).

Western blot analysis. The C4.4A-119 and C4.4A-277 antibodies in HCT116 each produced a band at around 70 kDa, and the absorbed antibodies eliminated these bands (Fig. 2A and B). On the other hand, the C4.4A GPI-P antibody in HCT116 produced doublet bands at 40 and 52 kDa (Fig. 2C), and the

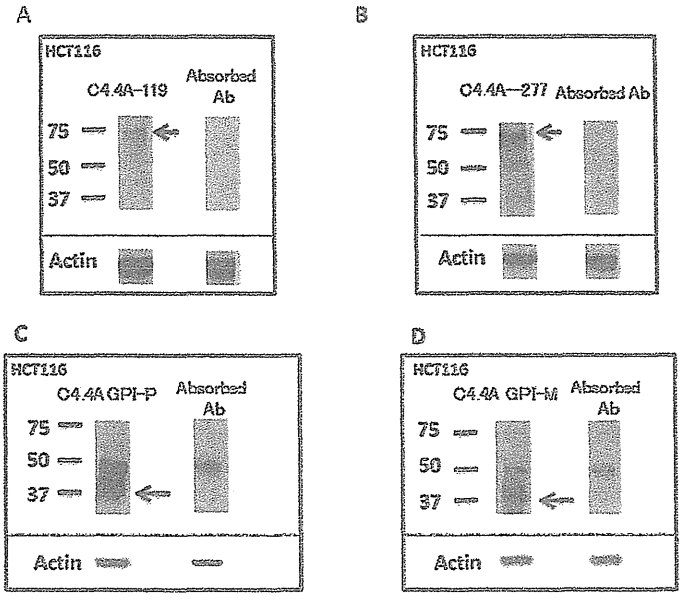

Figure 2. Western blot analysis for the C4.4A protein using lysates from HCT116 colon cancer cells. (A), C4.4A-119 antibody; (B), C4.4A-277 antibody; (C), C4.4A GPI-P antibody; (D), C4.4A GPI-M antibody. The arrows indicate the band corresponding to the C4.4A protein.

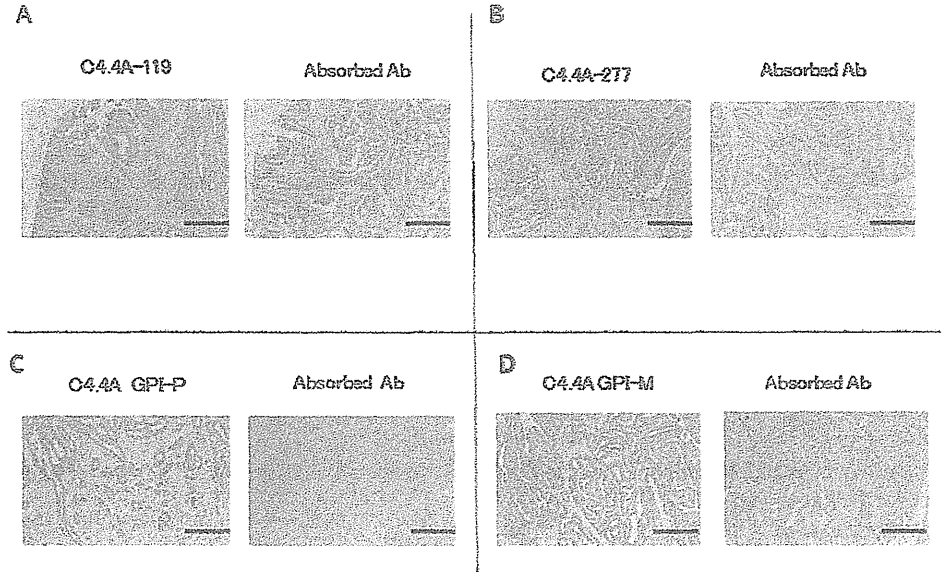

Figure 3. Absorption test on CRC tissues. (A), C4.4A-119 antibody; (B), C4.4A-277 antibody; (C), C4.4A GPI-P antibody; and (D), C4.4A GPI-M antibody. The scale bars indicate 500 μm (A-D).

absorbed antibody abolished a band at 40 kDa, which can be visualized on the tissue sections; similar results were observed with the C4.4A GPI-M antibody (Fig. 2D).

Immunohistochemistry. The C4.4A antibodies yielded positive staining for the C4.4A protein on tumor cells in CRC tissue specimens, and the pre-absorbed antibodies abolished this staining (Fig. 3).

Localization of C4.4A and positive staining rate in CRC tissues with each antibody. Immunohistochemistry revealed that the C4.4A protein was differently detected by each antibody in terms of intra-cellular and intra-tumoral locations, and positive staining rate. Using the C4.4A-119 antibody, positive staining was noted in 17 of 33 CRC cases (51.5%); relatively weak cytoplasmic staining was observed in the tumor cells, irrespective of location in the tumor body, i.e., superficial to intermediate area or invasive front (Fig. 4A). With the C4.4A-277 antibody, 29 of 33 CRC samples (87.9%) were positive for cytoplasmic C4.4A, and staining was observed at both the invasive front and superficial to intermediate portions (Fig. 4A); membranous staining was generally not evident, but weak positive staining

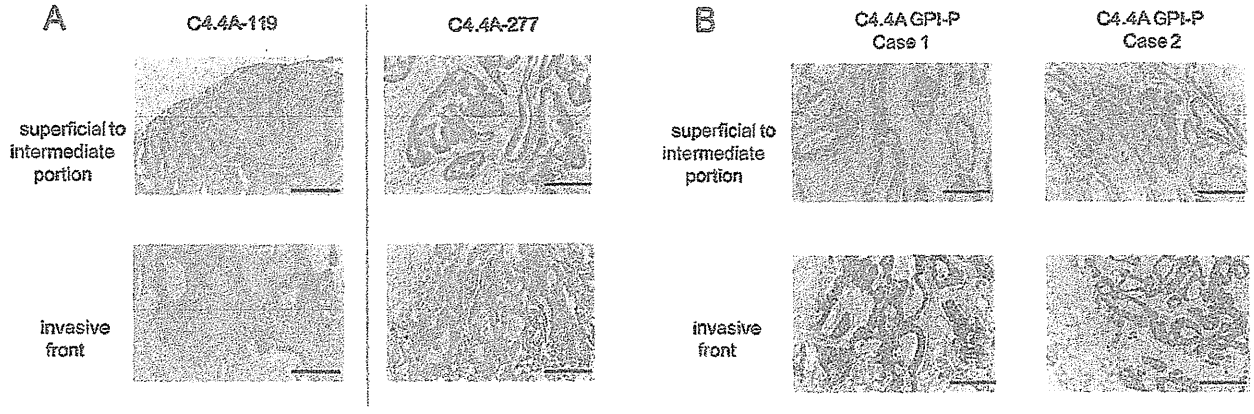

Figure 4. Immunohistochemistry of C4.4A at either a superficial to intermediate portion of the cancer body or at the invasive front of CRC tissue. (A), Representative CRC samples stained with the C4.4A-119 antibody, the C4.4A-277 antibody; and (B), the C4.4A GPI-P antibody. The scale bars indicate 200 μm (A and B).

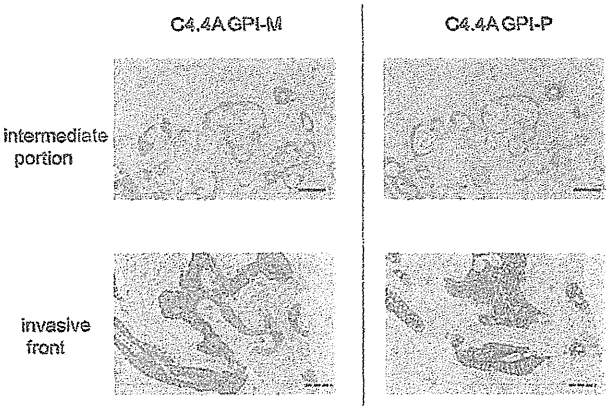

Figure 5. Immunohistochemistry of C4.4A using GPI-related antibodies. Serial sections stained with the C4.4A GPI-M antibody and the C4.4A GPI-P antibody showed identical patterns of C4.4A-positive cells in the cancer glands. Identical heterogeneous C4.4A expression patterns were also noted at the intermediate portion of the cancer body. The scale bars indicate 100 μm. A membranous expression pattern was observed at tumor invasive fronts with each antibody. The dotted scale bars indicate 50 μm.

was occasionally observed in only a portion of the cancer body. On the other hand, the C4.4A GPI-P antibody produced intense membranous staining at the invasive front in 11 of 33 CRC cases (33.3%), but this staining was usually not found at the superficial to intermediate portions (Fig. 4B).

The C4.4A GPI-M antibody showed a staining pattern similar to that produced by the C4.4A GPI-P antibody (Fig. 5). Staining by both GPI-related antibodies in serial sections revealed identical heterogeneous C4.4A expression patterns at the intermediate portion of the cancer body. The C4.4A GPI-M antibody also provided intense membranous staining in the tumor cells, only at the invasive front.

Discussion

In this study, we used four specific antibodies against the C4.4A protein, three of which were newly produced. Antibody specificities were verified by absorption tests, and efficacies by both western blot analysis and immunohistochemistry. The use of these distinct antibodies revealed several isoforms of the C4.4A protein, which differed in terms of molecular weight, intra-tumoral location, and intra-cellular localization. Western blot analysis revealed the existence of at least two isoforms: a long form of ~70 kDa, and a short form of ~40 kDa. This finding is consistent with the report by Paret *et al* that the recombinant C4.4A protein is digested by trypsin treatment from a long form of over 70 kDa to a proteolytic fragment of 40 kDa (9). Hansen *et al* also observed that both a long form (67 kDa) and short form (40 kDa) were present in the normal esophageal epithelium and at the superficial portion of the cancer body of the esophagus, whereas the short form of ~40 kDa was predominant in the invasive front of the cancer body (16).

In the present study, we found that the C4.4A-119 and C4.4A-277 antibodies reacted with the long form of C4.4A (70 kDa) and exhibited mainly cytoplasmic intra-cellular localization, irrespective of intra-tumoral location. In the tested CRC cases,

Table I. Detection of C4.4A expression by C4.4A antibodies.

	C4.4A-119	C4.4A-277	C4.4 GPI-P	C4.4 GPI-M
Positive rate in CRC tissue	51.5%	87.9%	33.3%	33.3%
Intra-cellular localization	Cytoplasm	Cytoplasm (occasionally plasma membrane)	Plasma membrane	Plasma membrane
Intra-tumor localization	All layers	All layers	Limited to invasive front	Limited to invasive front
Molecular weight	70 kDa	70 kDa	40 kDa	40 kDa

the C4.4A-119 and C4.4A-277 antibodies showed positive rates of 51.5% and 87.9%, respectively, indicating that cytoplasmic C4.4A was relatively frequently present in CRC tissues. Paret *et al* (9) previously used an antibody created with immunogens from two different portions of C4.4A (amino acids 278-302 and 119-138), and showed C4.4A expression in more than 80% of CRC tissue samples. Another study on C4.4A expression in esophageal squamous cell carcinoma (ESCC) showed a 100% detection rate (14 of 14 ESCC cases) using an antibody that recognizes the Domain III portion of the C4.4A molecule (5,16). These findings suggest that C4.4A could be a sensitive marker for CRC and ESCC when using the specific antibodies with high C4.4A detection rates.

On the other hand, we found that the C4.4A GPI-P antibody detected mainly membranous C4.4A at the invasive front of CRC tissues, at a lower rate of 33.3%. These findings suggest that, although cytoplasmic C4.4A is commonly detected in CRC tissues, only certain CRCs expressed membranous C4.4A. We hypothesize that the membranous type of C4.4A is functionally important and of clinical significance; it is possible that C4.4A on the plasma membrane could play a crucial role in invasion and metastasis. We previously reported that membranous C4.4A was linked to venous invasion, and associated with poor prognosis (especially hematogenous metastasis) in CRC (11). Moreover, we recently found that membranous C4.4A was tightly linked to EMT (epithelial-mesenchymal transition) change, and associated with tumor budding (17), a putative hallmark of cell invasion of CRC (18,19).

To explore whether the GPI anchor sequence was essential for detecting membranous C4.4A at the invasive front, we developed the novel monoclonal antibody C4.4A GPI-M. The antibody detected a membranous C4.4A expression pattern at the invasive front, similar to that shown by the C4.4A GPI-P antibody. Both C4.4A GPI-P and C4.4A GPI-M antibodies produced a band at around 40 kDa. These findings suggest that the C4.4A protein may exist as a proteolytic fragment on the plasma membrane in a subset of CRC. Based on these results, we concluded that the GPI anchor signaling sequence is essential for detecting membranous C4.4A at the invasive front. The present findings also suggest that C4.4A might be digested into the short form at the invasive front of CRC when it links to the plasma membrane via the GPI anchor.

In conclusion, as summarized in Table I, we found that the majority of CRC tissues expressed cytoplasmic C4.4A, and a subset of CRCs displayed C4.4A on the plasma membrane. Both the C4.4A GPI-M antibody and the C4.4A GPI-P antibody exhibited membranous expression patterns, suggesting that the GPI anchor signaling sequence is essential for detecting membranous C4.4A at the invasive front.

Acknowledgements

This work was supported by a Grant-in-Aid for Cancer Research from the Ministry of Education, Science, Sports, and Culture Technology, Japan, to H.Y.

References

1. Claas C, Herrmann K, Matzku S, Möller P and Zöller M: Developmentally regulated expression of metastasis-associated antigens in the rat. Cell Growth Differ 7: 663-678, 1996.
2. Matzku S, Wenzel A, Liu S and Zöller M: Antigenic differences between metastatic and nonmetastatic BSp73 rat tumor variants characterized by monoclonal antibodies. Cancer Res 49: 1294-1299, 1989.
3. Würfel J, Seiter S, Stassar M, *et al*: Cloning of the human homologue of the metastasis-associated rat C4.4A. Gene 262: 35-41, 2001.
4. Rösel M, Claas C, Seiter S, Herlevsen M and Zöller M: Cloning and functional characterization of a new phosphatidyl-inositol anchored molecule of a metastasizing rat pancreatic tumor. Oncogene 17: 1989-2002, 1998.
5. Hansen LV, Gårdsvoll H, Nielsen BS, *et al*: Structural analysis and tissue localization of human C4.4A: a protein homologue of the urokinase receptor. Biochem J 380: 845-857, 2004.
6. Hansen LV, Skov BG, Ploug M and Pappot H: Tumour cell expression of C4.4A, a structural homologue of the urokinase receptor, correlates with poor prognosis in non-small cell lung cancer. Lung Cancer 58: 260-266, 2007.
7. Seiter S, Stassar M, Rappl G, Reinhold U, Tilgen W and Zöller M: Upregulation of C4.4A expression during progression of melanoma. J Invest Dermatol 116: 344-347, 2001.
8. Fletcher G, Patel S, Tyson K, *et al*: hAG-2 and hAG-3, human homologues of genes involved in differentiation, are associated with oestrogen receptor-positive breast tumours and interact with metastasis gene C4.4a and dystroglycan. Br J Cancer 88: 579-585, 2003.
9. Paret C, Hildebrand D, Weitz J, *et al*: C4.4A as a candidate marker in the diagnosis of colorectal cancer. Br J Cancer 97: 1146-1156, 2007.
10. Smith BA, Kennedy WJ, Harnden P, Selby PJ, Trejdosiewicz LK and Southgate J: Identification of genes involved in human urothelial cell - matrix interactions: implications for the progression pathways of malignant urothelium. Cancer Res 61: 1678-1685, 2001.
11. Konishi K, Yamamoto H, Mimori K, *et al*: Expression of C4.4A at the invasive front is a novel prognostic marker for disease recurrence of colorectal cancer. Cancer Sci 101: 2269-2277, 2010.
12. Noura S, Yamamoto H, Ohnishi T, *et al*: Comparative detection of lymph node micrometastases of stage II colorectal cancer by reverse transcriptase polymerase chain reaction and immunohistochemistry. J Clin Oncol 20: 4232-4241, 2002.
13. Yamamoto H, Kondo M, Nakamori S, *et al*: JTE-522, a cyclooxygenase-2 inhibitor, is an effective chemopreventive agent against rat experimental liver fibrosis. Gastroenterology 125: 556-571, 2003.
14. Takemasa I, Yamamoto H, Sekimoto M, *et al*: Overexpression of CDC25B phosphatase as a novel marker of poor prognosis of human colorectal carcinoma. Cancer Res 60: 3043-3050, 2000.
15. Yamamoto H, Soh JW, Shirin H, *et al*: Comparative effects of overexpression of $p27^{Kip1}$ and $p21^{Cip1/Waf1}$ on growth and differentiation in human colon carcinoma cells. Oncogene 18: 103-115, 1999.
16. Hansen LV, Laerum OD, Illemann M, Nielsen BS and Ploug M: Altered expression of the urokinase receptor homologue, C4.4A, in invasive areas of human esophageal squamous cell carcinoma. Int J Cancer 122: 734-741, 2008.
17. Oshiro R, Yamamoto H, Takahashi H, *et al*: C4.4A is associated with tumor budding and epithelial-mesenchymal transition of colorectal cancer. Cancer Sci 103: 1155-1164, 2012.
18. Hase K, Shatney C, Johnson D, Trollope M and Vierra M: Prognostic value of tumor budding in patients with colorectal cancer. Dis Colon Rectum 36: 627-635, 1993.
19. Ueno H, Murphy J, Jass J, Mochizuki H and Talbot I: Tumour-budding as an index to estimate the potential of aggressiveness in rectal cancer. Histopathology 40: 127-132, 2002.

JACS
JOURNAL OF THE AMERICAN CHEMICAL SOCIETY

Communication

pubs.acs.org/JACS

Bioactive Polymeric Metallosomes Self-Assembled through Block Copolymer–Metal Complexation

Kensuke Osada,[†,∥] Horacio Cabral,[‡,∥] Yuki Mochida,[‡] Sangeun Lee,[‡] Kazuya Nagata,[§] Tetsuya Matsuura,[†] Megumi Yamamoto,[‡] Yasutaka Anraku,[†] Akihiro Kishimura,[†] Nobuhiro Nishiyama,[§] and Kazunori Kataoka*[,†,‡,§]

[†]Department of Materials Engineering and [‡]Department of Bioengineering, Graduate School of Engineering, The University of Tokyo, 7-3-1 Hongo, Bunkyo-ku, Tokyo 113-8656, Japan

[§]Division of Clinical Biotechnology, Center for Disease Biology and Integrative Medicine, Graduate School of Medicine, The University of Tokyo, 7-3-1 Hongo, Bunkyo-ku, Tokyo 113-8656, Japan

Supporting Information

ABSTRACT: Spontaneous formation of polymeric metallosomes with uniform size (~100 nm) was found to occur in aqueous medium through the reaction of an anticancer agent, (1,2-diaminocyclohexane)platinum(II) (DACHPt), with a Y-shaped block copolymer of ω-cholesteroyl-poly(L-glutamic acid) and two-armed poly(ethylene glycol) (PEGasus-PLGA-Chole). Circular dichroism spectrum measurements revealed that the PLGA segment forms an α-helix structure within the metallosomes, suggesting that secondary-structure formation of metallocomplexed PLGA segment may drive the self-assembly of the system into vesicular structure. These metallosomes can encapsulate water-soluble fluorescent macromolecules into their inner aqueous phase and eventually deliver them selectively into tumor tissues in mice, owing to the prolonged blood circulation. Accordingly, fluorescent imaging of the tumor was successfully demonstrated along with an appreciable antitumor activity by DACHPt moieties retained in the vesicular wall of the metallosomes, indicating the potential of metallosomes as multifunctional drug carriers.

Supramolecular architectures constructed through a self-assembly of block copolymers are attracting much interest because of their versatile morphologies. In particular, studies on vesicles (also known as polymersomes) have become a key area of focus because of interest in the study of their formation mechanisms,[1−4] morphology tuning,[5] and their potential as delivery carriers.[6] Various types of polymersomes have been developed from various interactions,[6] such as hydrophobic interactions by amphiphilic block copolymers, where the morphology can be modulated through ion−polymer complexation,[5,7] and electrostatic interactions from oppositely charged block copolymers.[8,9] The metal coordination bond is interesting as the membrane properties of polymersomes can be changed within water by a ligand-exchange reaction. This property is important for biomedical applications because the controlled release of loaded materials in the polymersomes is a crucial issue when the polymersomes are utilized as carriers to deliver therapeutic agents. Here, we succeeded to prepare spontaneous polymersome formation in water triggered by metal coordination bond, namely metallosomes, enabling the controlled release property of the cargos at the target site in the body. The metallosomes are formed between the aqueous complex of (1,2-diaminocyclohexane)platinum(II) (DACHPt), the active compound of the widely used platinum-based anticancer drug oxaliplatin,[10,11] and the carboxylic moieties of the poly(L-glutamic acid) (PLGA) segment of two-armed PEG-*b*-PLGA-cholesterol (PEGasus-PLGA-Chole), comprising the biocompatible components. The architecture of the metallosomes provides considerable storage capacity for water-soluble molecules within its inner water phase and, therefore, has tremendous potential for encapsulation and controlled delivery of water-soluble agents together with DACHPt moieties in the vesicular wall as anticancer agents. These metallosomes work as multifunctional drug carriers demonstrating tumor imaging through encapsulated fluorescent molecules within the inner aqueous phase along with appreciable antitumor activity.

The self-assembly occurred in water through complexation of DACHPt and PEGasus-PLGA-Chole block copolymers (PEGasus; 20 000 Da, degree of polymerization (DP) of PLGA; 20) (Figure 1a). A dynamic light scattering (DLS) measurement for this assembly showed a size of approximately 100 nm with narrow unimodal size distribution (Figure 1b). The structure of the assembly was investigated using transmission electron microscopy (TEM). The TEM image shown in Figure 1c was consistent with hollow vesicular structures, although collapse and aggregation occurred presumably during the vacuum treatment of the samples. Moreover, the vesicular assembly with clear thin membrane structure was observed in a cryogenic phase-contrast TEM (cryo-PCTEM) image (Figure 2a(i)), further supporting the formation of vesicles.

Given the vesicular nature of the assembly, it is possible to load hydrophilic molecules into its inner water space. Accordingly, PEGasus-PLGA-Chole and DACHPt were assembled in the presence of dextran labeled with FITC (FITC-dextran; 10 000 Da), and subsequently the solution was ultrafiltered to eliminate the FITC-dextran that was outside the assembly. The incorporation of the FITC-dextran into the

Received: May 11, 2012
Published: July 27, 2012

dx.doi.org/10.1021/ja304615y | J. Am. Chem. Soc. 2012, 134, 13172−13175

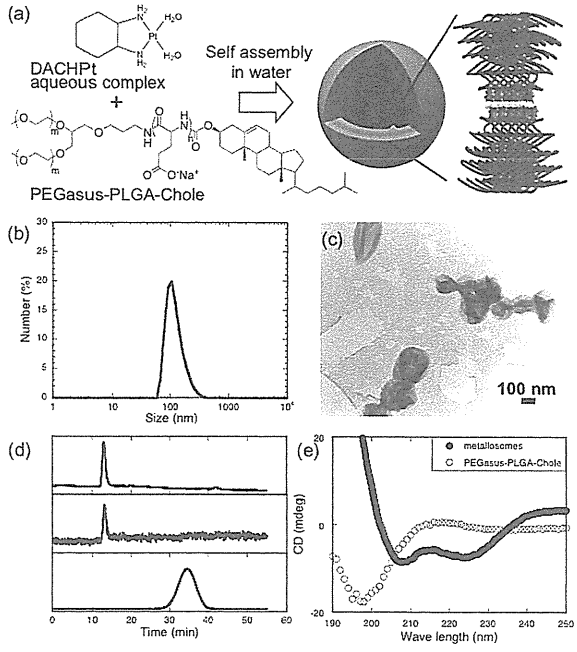

Figure 1. Formation and structure evaluations of metallosomes. (a) Schematic diagram of the proposed self-assembly of metallosomes through the formation of a metal complex between a Pt atom in the DACHPt and the carboxylic moiety of PLGA segment. (b) Size distribution of metallosomes measured by DLS. (c) Transmission electron micrograph of metallosomes stained with uranyl acetate. (d) Gel permeation chromatograms of FITC-dextran-loaded metallosomes (upper: UV absorption; center: fluorescence detection) and free FITC-dextran (lower: fluorescence detection). (e) CD spectra of metallosomes and PEGasus-PLGA-Chole block copolymer measured at neutral pH.

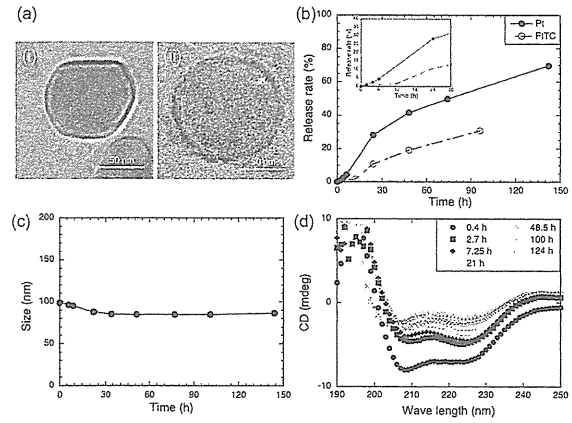

Figure 2. Release profiles of metallosomes under the physiological conditions (10 mM phosphate buffer (PB) plus 150 mM NaCl). (a) Cryogenic PCTEM images of metallosomes of (i) 0 h incubation and (ii) after 48 h incubation. Thickness of the vesicular membrane (indicated by arrows) was measured to be 6.3 nm in average from 11 independent metallosomes. (b) Release profiles of Pt complexes from the metallosomes and FITC-dextran from FITC-dextran-loaded metallosomes. Inset indicates the release profiles of early stage. Data are mean ± SD of n = 3. (c) Size change of metallosomes with incubation time determined by DLS. (d) Variation of CD spectra of the metallosomes with incubation time.

assembly was confirmed by gel permeation chromatography (GPC). The fluorescence of the incorporated FITC-dextran was determined at the same elution time as that of the assembly, whereas the free FITC-dextran appeared at a much later elution time (Figure 1d). This provided evidence for the coexistence of the FITC-dextran and the assembly. This result confirmed the vesicular nature of the assembly with inner water space; thus, it was named as "metallosome". Concurrently, the result indicates high potential of the metallosome as a reservoir for hydrophilic agents.

Formation of vesicular structures indicates that there may be particular structures of the constituent block copolymer that stabilize a lamellar phase of the vesicular membrane. Circular dichroism (CD) analysis revealed that the PLGA segment adopts an α-helix structure in metallosomes (Figure 1e, closed circle). PLGA is a well-known polypeptide that forms an α-helix under acidic conditions or when substituting side chains,[12] while adopting a random coil structure at neutral pH, as demonstrated by the CD spectrum of free PEGasus-PLGA-Chole block copolymer in the solution (Figure 1e, open circle). Binding of DACHPt to carboxylic moieties of PLGA induced α-helix formation even under neutral conditions, presumably because of decreased intramolecular electrostatic repulsion of the carboxylic moieties. Considering the inherent nature of cylindrical α-helices to pack laterally with each other[13−16] favoring formation of flat membrane and the nature of PEG and PLGA blocks to segregate, possible orientations of α-helices in the metallosome membrane are α-helices aligned (i) in an antiparallel manner to form a single layer or (ii) in a parallel manner to form double layers, with cholesterol (Chole) groups buried between the α-helix layers. From the viewpoint of free energy, the parallel alignment (ii) would be more favorable because hydrophobic Chole groups attached to the ω-end of the block copolymers can assemble between the α-helix double layers within a hydrophobic environment as schematically depicted in Figure 1a. Furthermore, Chole groups can assemble to form a cholesteric liquid crystal phase,[17,18] which could provide additional stability to the α-helix double layers. Moreover, well-controlled polymer segment lengths with narrow molecular weight distribution (M_w/M_n = 1.05) would facilitate interface alignment and lamellar formation. Assuming the parallel alignment as the most plausible structure, a molecular model calculated the double-layer thickness to be 7.0 nm [Supporting Information (SI)]. The measured thickness of the peripheral rings structure of the metallosome in cryo-PCTEM images (Figure 2a) was determined to be 6.3 nm (n = 11), which is comparable to the value calculated with the molecular model. Note that the PEG layer was not observed in the cryo-PCTEM images because of low electron density. The presence of Chole and PEGasus moieties in the block copolymers plays a crucial role for the vesicular formation because the combination of DACHPt and PEG-PLGA-Chole (no-branched linear PEG) resulted in polymeric micelles (Figure S1a, SI) and the combination of DACHPt and PEGasus-PLGA (without Chole) failed to form vesicles (Figure S1b, SI). As the metallosomes are formed in water, PLGA-Chole parts generate strong cohesive forces because of the presence of hydrophobic Chole groups and DACHPt molecules and, thus, tend to coagulate to decrease the interface to water. However, large osmotic pressure from the hydrated two-armed PEGasus tends to expand the interface. Under such frustrated conditions, the ordered alignment as lamellar may be favored to balance steric repulsion from the PEGasus layer and

coagulation of the α-helical cylinder with Chole moiety at ω-end.

The properties of metallosomes as drug carriers were then investigated. The amount of DACHPt in the metallosomes was determined by inductively coupled plasma-mass spectroscopy (ICP-MS) to be 10 wt % of the product. This is approximately 50% of the carboxylate moieties of PLGA complexed to DACHPt. The binding of DACHPt to PLGA is stable in distilled water but may be gradually cleaved under physiological NaCl conditions through the exchange reaction between chloride ions in the medium and the carboxylate group of the PLGA.[19] Thus metallosomes release the active Pt complexes in a sustained manner, achieving a discharge of more than 50% of the DACHPt after 72 h (Figure 2b inset). In contrast, a clear induction period during the first 12 h was observed in the release profile of Alexa 680-dextran (10 000 Da) incorporated in the interior of the metallosomes (Figure 2b). Presumably, the membrane of metallosomes is still not permeable to Alexa 680-dextran in the early stage until the release of a critical amount of Pt complex. This results in an increase in the threshold molecular weight cutoff of the membrane permeability, and ultimately enabling Alexa 680-dextran to penetrate the membrane. The initial induction phase is apparently an advantage when targeting solid tumors, as the release of the cargo in the inner phase is expected to occur after the vesicles reach the tumor tissue. Moreover, the induction period in dextran release suggests that the vesicular structure is assumed to be stable even after the substantial release of the Pt complex. Indeed the observation of the constant size of approximately 80 to 90 nm diameter for a prolonged time period at physiological NaCl concentration (Figure 2c) is consistent with the maintenance of the vesicular structure. Furthermore, the cryo-PCTEM images of the metallosomes incubated 48 h under physiological conditions revealed the presence of the vesicular structure (Figure 2a(ii)). CD intensity for the α-helix decreased with incubation time in physiological conditions (Figure 2d), indicating that the PLGA segments in the metallosome gradually underwent a transition from α-helix to random coil with the release of DACHPt. Yet, worthy to note is that the characteristic α-helix spectra still remained even after prolonged incubation, suggesting a crucial role of α-helices in maintaining the vesicular structure.

The small size of approximately 100 nm with PEGylated palisade of the metallosomes is a substantial advantage to attain prolonged blood circulation and ultimately increases the accumulation of metallosomes in tumors through passive targeting based on the EPR effect.[20] Moreover, metallosomes might be very valuable for the systemic codelivery of both the Pt complex and encapsulated agents in the hollow water space. Thus, blood circulation of the FITC-dextran-loaded metallosomes was evaluated through the detection of both Pt (Figure 3a) and FITC fluorescence (Figure 3b). The results clearly exhibited prolonged retention in the bloodstream for both species. Alternatively, both free oxaliplatin, which is an oxalate complex of DACHPt (Figure 3a), and free FITC-dextran (Figure 3b) were rapidly cleared from the bloodstream. Co-injection of free FITC-dextran with empty metallosomes revealed no improved plasma retention compared to the single injection (Figure 3b), excluding the possibility that the FITC-dextran adsorption to the metallosome surface brought the longevity in blood circulation. Eventually, the augmented bioavailability of metallosomes and the EPR effect enabled an increased accumulation of both DACHPt and FITC-dextran

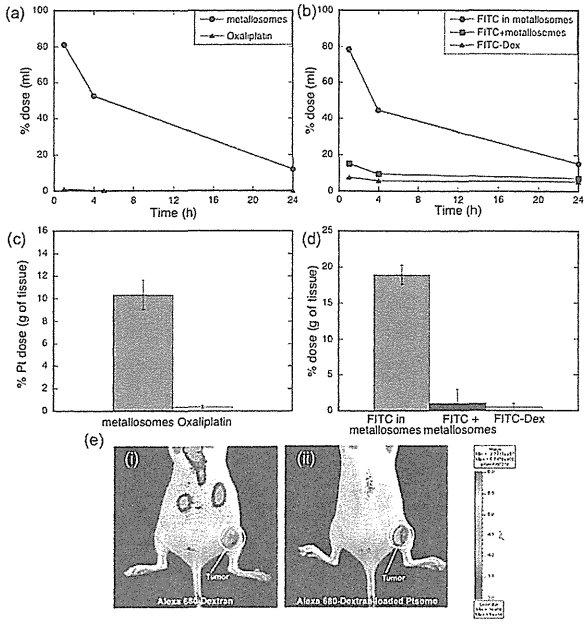

Figure 3. *In vivo* performance of metallosomes through i.v. injection. (a) Plasma clearance of Pt after injection of oxaliplatin and metallosomes. (b) Plasma clearance of free FITC-dextran, free FITC-dextran coinjected with metallosomes, and FITC-dextran-loaded metallosomes. (c) Tumor accumulation of Pt 24 h after injection for metallosomes and oxaliplatin. (d) Tumor accumulation of FITC-dextran 24 h after injection for FITC-dextran-loaded metallosomes, free FITC-dextran co-injected with metallosomes, and free FITC-dextran. (e) *In vivo* fluorescent imaging of free Alexa 680-dextran (i) and Alexa 680-dextran-loaded metallosomes (ii) 24 h after injection. Data are mean ± SD of $n = 6$.

into subcutaneous colon adenocarcinoma 26 (C26) tumors (Figure 3c,d), confirming the high potency of the metallosomes as the systemic multifunctional carrier.

In vivo noninvasive imaging of nanocarriers is plausible for determining their tissue selectivity and estimating their therapeutic and diagnostic potentials. In this regard, the preferential tumor accumulation of Alexa 680-dextran was clearly observed by *in vivo* near-infrared fluorescence imaging after the injection of Alexa 680-dextran-loaded metallosomes (Figure 3e). In contrast, the signal of Alexa 680-dextran injected in the free form mainly appeared at the kidneys, visually confirming the high capacity of metallosome as the nanocarrier directing encapsulated substances to solid tumors.

This elevated tumor accumulation of metallosomes is expected to improve the antitumor activity of the incorporated platinum drug, since DACHPt complexes can exert their cytotoxicity after being released from the metallosomes as observed in *in vitro* studies (Table S1, SI). We studied the antitumor activity of oxaliplatin and the metallosomes in C-26-bearing mice through intravenous (i.v.) injection. For free oxaliplatin, no inhibition of the tumor growth was observed at any dose in this condition (Figure 4a). Moreover, the mice injected with 10 mg/kg of oxaliplatin presented toxic death after the third injection (Figure 4b). Mice treated with 6 mg/kg of metallosomes achieved considerable reduction in the tumor growth rate ($p < 0.005$ at day 14) (Figure 4a), which was comparable to the previously reported data obtained for the DACHPt loaded micelles undergoing clinical trial,[21] because of